In conclusion, the automatic, highly sensitive HBsAg CLEIA Lumipulse HBsAg-HQ assay is a very convenient and precise assay for HBV monitoring in clinical practice.

ACKNOWLEDGMENTS

This study was supported by a grant-in-aid from the Ministry of Education, Culture, Sports, Science, and Technology and a grant-in-aid from the Ministry of Health, Labor, and Welfare of Japan.

The authors declare no conflicts of interest.

REFERENCES

1. **Pan CQ, Zhang JX.** 2005. Natural history and clinical consequences of hepatitis B virus infection. Int. J. Med. Sci. 2:36–40.
2. **Kohmoto M, Enomoto M, Tamori A, Habu D, Takeda T, Kawada N, Sakaguchi H, Seki S, Shiomi S, Nishiguchi S.** 2005. Quantitative detection of hepatitis B surface antigen by chemiluminescent microparticle immunoassay during lamivudine treatment of chronic hepatitis B virus carriers. J. Med. Virol. 75:235–239.
3. **Chan HL, Wong VW, Tse AM, Tse CH, Chim AM, Chan HY, Wong GL, Sung JJ.** 2007. Serum hepatitis B surface antigen quantitation can reflect hepatitis B virus in the liver and predict treatment response. Clin. Gastroenterol. Hepatol. 5:1462–1468.
4. **Werle B, Cinquin K, Marcellin P, Pol S, Maynard M, Trépo C, Zoulim F.** 2004. Evolution of hepatitis B viral load and viral genome sequence during adefovir dipivoxil therapy. J. Viral Hepat. 11:74–83.
5. **Wursthorn K, Lutgehetmann M, Dandri M, Volz T, Buggisch P, Zollner B, Longerich T, Schirmacher P, Metzler F, Zankel M, Fischer C, Currie G, Brosgart C, Petersen J.** 2006. Peginterferon alpha-2b plus adefovir induce strong cccDNA decline and HBsAg reduction in patients with chronic hepatitis B. Hepatology 44:675–684.
6. **Brunetto MR, Moriconi F, Bonino F, Lau GK, Farci P, Yurdaydin C, Piratvisuth T, Luo K, Wang Y, Hadziyannis S, Wolf E, McCloud P, Batrla R, Marcellin P.** 2009. Hepatitis B virus surface antigen levels: a guide to sustained response to peginterferon alfa-2a in HBeAg-negative chronic hepatitis B. Hepatology 49:1141–1150.
7. **Chen CH, Lee CM, Wang JH, Tung HD, Hung CH, Lu SN.** 2004. Correlation of quantitative assay of hepatitis B surface antigen and HBV DNA levels in asymptomatic hepatitis B virus carriers. Eur. J. Gastroenterol. Hepatol. 16:1213–1218.
8. **Deguchi M, Yamashita N, Kagita M, Asari S, Iwatani Y, Tsuchida T, Iinuma K, Mushahwar IK.** 2004. Quantitation of hepatitis B surface antigen by an automated chemiluminescent microparticle immunoassay. J. Virol. Methods 115:217–222.
9. **Martinot-Peignoux M, Maylin S, Moucari R, Ripault MP, Boyer N, Cardoso AC, Giuily N, Castelnau C, Pouteau M, Stern C, Aupérin A, Bedossa P, Asselah T, Marcellin P.** 2009. Virological response at 4 weeks to predict outcome of hepatitis C treatment with pegylated interferon and ribavirin. Antivir. Ther. 14:501–511.
10. **Matsubara N, Kusano O, Sugamata Y, Itoh T, Mizuii M, Tanaka J, Yoshizawa H.** 2009. A novel hepatitis B virus surface antigen immunoassay as sensitive as hepatitis B virus nucleic acid testing in detecting early infection. Transfusion 49:585–595.
11. **Shinkai N, Tanaka Y, Matsuura K, Kani S, Naganuma H, Mizokami M.** 2010. Evaluation and application of a newly developed highly sensitive HBsAg chemiluminescent enzyme immunoassay for chronic hepatitis B patients. Rinsho Byori 58:1078–1084. (Article in Japanese.)
12. **Kimura T, Rokuhara A, Sakamoto Y, Yagi S, Tanaka E, Kiyosawa K, Maki N.** 2002. Sensitive enzyme immunoassay for hepatitis B virus core-related antigens and their correlation to virus load. J. Clin. Microbiol. 40:439–445.
13. **Wong DK, Tanaka Y, Lai CL, Mizokami M, Fung J, Yuen MF.** 2007. Hepatitis B virus core-related antigens as markers for monitoring chronic hepatitis B infection. J. Clin. Microbiol. 45:3942–3947.
14. **Moucari R, Korevaar A, Lada O, Martinot-Peignoux M, Boyer N, Mackiewicz V, Dauvergne A, Cardoso AC, Asselah T, Nicolas-Chanoine MH, Vidaud M, Valla D, Bedossa P, Marcellin P.** 2009. High rates of HBsAg seroconversion in HBeAg-positive chronic hepatitis B patients responding to interferon: a long-term follow-up study. J. Hepatol. 50:1084–1092.
15. **van Zonneveld M, Honkoop P, Hansen BE, Niesters HG, Darwish Murad S, de Man RA, Schalm SW, Janssen HL.** 2004. Long-term follow-up of alpha-interferon treatment of patients with chronic hepatitis B. Hepatology 39:804–810.
16. **Simonetti J, Bulkow L, McMahon BJ, Homan C, Snowball M, Negus S, Williams J, Livingston SE.** 2010. Clearance of hepatitis B surface antigen and risk of hepatocellular carcinoma in a cohort chronically infected with hepatitis B virus. Hepatology 51:1531–1537.
17. **Yuen MF, Wong DK, Fung J, Ip P, But D, Hung I, Lau K, Yuen JC, Lai CL.** 2008. HBsAg seroclearance in chronic hepatitis B in Asian patients: replicative level and risk of hepatocellular carcinoma. Gastroenterology 135:1192–1199.
18. **Suzuki F, Miyakoshi H, Kobayashi M, Kumada H.** 2009. Correlation between serum hepatitis B virus core-related antigen and intrahepatic covalently closed circular DNA in chronic hepatitis B patients. J. Med. Virol. 81:27–33.
19. **Shinkai N, Tanaka Y, Orito E, Ito K, Ohno T, Hirashima N, Hasegawa I, Sugauchi F, Ueda R, Mizokami M.** 2006. Measurement of hepatitis B virus core-related antigen as predicting factor for relapse after cessation of lamivudine therapy for chronic hepatitis B virus infection. Hepatol Res. 36:272–276.
20. **Hollinger FB.** 2008. Hepatitis B virus infection and transfusion medicine: science and the occult. Transfusion 48:1001–1026.
21. **Raimondo G, Pollicino T, Cacciola I, Squadrito G.** 2007. Occult hepatitis B virus infection. J. Hepatol. 46:160–170.
22. **van Hemert FJ, Zaaijer HL, Berkhout B, Lukashov VV.** 2008. Occult hepatitis B infection: an evolutionary scenario. Virol. J. 5:146. doi:10.1186/1743-422X-5-146.
23. **Dettori S, Candido A, Kondili LA, Chionne P, Taffon S, Genovese D, Iudicone P, Miceli M, Rapicetta M.** 2009. Identification of low HBV-DNA levels by nucleic acid amplification test (NAT) in blood donors. J. Infect. 59:128–133.
24. **Satake M, Taira R, Yugi H, Hino S, Kanemitsu K, Ikeda H, Tadokoro K.** 2007. Infectivity of blood components with low hepatitis B virus DNA levels identified in a lookback program. Transfusion 47:1197–1205.
25. **Fukushima N, Mizuta T, Tanaka M, Yokoo M, Ide M, Hisatomi T, Kuwahara N, Tomimasu R, Tsuneyoshi N, Funai N, Sueoka E.** 2009. Retrospective and prospective studies of hepatitis B virus reactivation in malignant lymphoma with occult HBV carrier. Ann. Oncol. 20:2013–2017.
26. **Law JK, Ho JK, Hoskins PJ, Erb SR, Steinbrecher UP, Yoshida EM.** 2005. Fatal reactivation of hepatitis B post-chemotherapy for lymphoma in a hepatitis B surface antigen-negative, hepatitis B core antibody-positive patient: potential implications for future prophylaxis recommendations. Leuk. Lymphoma 46:1085–1089.
27. **Pei SN, Chen CH, Lee CM, Wang MC, Ma MC, Hu TH, Kuo CY.** 2010. Reactivation of hepatitis B virus following rituximab-based regimens: a serious complication in both HBsAg-positive and HBsAg-negative patients. Ann. Hematol. 89:255–262.
28. **Wu JM, Huang YH, Lee PC, Lin HC, Lee SD.** 2009. Fatal reactivation of hepatitis B virus in a patient who was hepatitis B surface antigen negative and core antibody positive before receiving chemotherapy for non-Hodgkin lymphoma. J. Clin. Gastroenterol. 43:496–498.
29. **Yeo W, Chan TC, Leung NW, Lam WY, Mo FK, Chu MT, Chan HL, Hui EP, Lei KI, Mok TS, Chan PK.** 2009. Hepatitis B virus reactivation in lymphoma patients with prior resolved hepatitis B undergoing anticancer therapy with or without rituximab. J. Clin. Oncol. 27:605–611.
30. **Chen WN, Oon CJ.** 2000. Hepatitis B virus surface antigen (HBsAg) mutants in Singapore adults and vaccinated children with high anti-hepatitis B virus antibody levels but negative for HBsAg. J. Clin. Microbiol. 38:2793–2794.
31. **Wu C, Deng W, Deng L, Cao L, Qin B, Li S, Wang Y, Pei R, Yang D, Lu M, Chen X.** 2012. Amino acid substitutions at positions 122 and 145 of hepatitis B virus surface antigen (HBsAg) determine the antigenicity and immunogenicity of HBsAg and influence *in vivo* HBsAg clearance. J. Virol. 86:4658–4669.
32. **Oon CJ, Chen WN, Goh KT, Mesenas S, Ng HS, Chiang G, Tan C, Koh S, Teng SW, Toh I, Moh MC, Goo KS, Tan K, Leong AL, Tan GS.** 2002. Molecular characterization of hepatitis B virus surface antigen mutants in Singapore patients with hepatocellular carcinoma and hepatitis B virus carriers negative for HBsAg but positive for anti-HBs and anti-HBc. J. Gastroenterol. Hepatol. 17(Suppl):S491–S496.
33. **Coleman PF.** 2006. Detecting hepatitis B surface antigen mutants. Emerg. Infect. Dis. 12:198–203.

World Journal of Gastroenterology

Online Submissions: http://www.wjgnet.com/esps/
wjg@wjgnet.com
doi:10.3748/wjg.v19.i37.6214

World J Gastroenterol 2013 October 7; 19(37): 6214-6220
ISSN 1007-9327 (print) ISSN 2219-2840 (online)

BRIEF ARTICLE

Incidence and characteristics of HBV reactivation in hematological malignant patients in south Egypt

Abeer Elkady, Sahar Aboulfotuh, Elsayed Mostafa Ali, Douaa Sayed, Nashwa M Abdel-Aziz, Amany M Ali, Shuko Murakami, Sayuki Iijima, Yasuhito Tanaka

Abeer Elkady, Shuko Murakami, Sayuki Iijima, Yasuhito Tanaka, Department of Virology and Liver Unit, Nagoya City University Graduate School of Medical Sciences, Nagoya 467-8601, Japan
Abeer Elkady, Department of Clinical and Chemical Pathology, Medical School of South Valley University, Qena 83523, Egypt
Sahar Aboulfotuh, Department of Clinical and Chemical Pathology, Medical School of Sohag University, Sohag 82524, Egypt
Elsayed Mostafa Ali, Department of Medical Oncology, Medical School of Sohag University, Sohag 82524, Egypt
Douaa Sayed, Department of Clinical and Chemical Pathology, South Egypt Cancer Institute, Assuti 71515, Egypt
Nashwa M Abdel-Aziz, Amany M Ali, Department of Medical Oncology, South Egypt Cancer Institue, 71515 Assuit, Egypt
Author contributions: Elkady A and Tanaka Y designed the study, directed its implementation, supervised all of the field activities, and contributed to the analysis and interpretation of the data as well as to the redaction of the manuscript; Ali EM, Aboulfotuh S, Sayed D, Abdel-Aziz NM, and Ali AM contributed to the collection of the materials and patient data; Murakami S and Iijima S contributed to the analysis and interpretation of the data.
Supported by The Grant for National Center For Global Health and Medicine (22A-9); a Grant-in-Aid form Japan Society for the Promotion of Science (JSPS) Fellows (21.09355) and a Grant-in-Aid form the Ministry of Health, Labour and Welfare of Japan
Correspondence to: Yasuhito Tanaka, MD, PhD, Department of Virology and Liver Unit, Nagoya City University Graduate School of Medical Sciences, Nagoya 467-8601, Japan. ytanaka@med.nagoya-cu.ac.jp
Telephone: +81-52-8538191 Fax: +81-52-8420021
Received: April 27, 2013 Revised: July 24, 2013
Accepted: August 4, 2013
Published online: October 7, 2013

Abstract

AIM: To investigate characteristics of hepatitis B virus (HBV) implicated in HBV reactivation in patients with hematological malignancies receiving immunosuppressive therapy.

METHODS: Serum samples were collected from 53 patients with hematological malignancies negative for hepatitis B surface antigen (HBsAg) before the start of and throughout the chemotherapy course. HBV reactivation was diagnosed when the HBsAg status changed from negative to positive after the initiation of chemotherapy and/or when HBV DNA was detected by real-time detection polymerase chain reaction (RTD-PCR). For detecting the serological markers of HBV infection, HBsAg as well as antibodies to the core antigen (anti-HBc) and to the surface antigen were measured in the sera by CEIA. Nucleic acids were extracted from sera, and HBV DNA sequences spanning the S gene were amplified by RTD-PCR. The extracted DNA was further subjected to PCR to amplify the complete genome as well as the specific genomic sequences bearing the enhancer Ⅱ/core promoter/pre-core/core regions (nt 1628-2364). Amplicons were sequenced directly.

RESULTS: Thirty-five (66%) of the 53 HBsAg-negative patients were found to be negative serologically for anti-HBc, and the remaining 18 (34%) patients were positive for anti-HBc. Five of the 53 (9.4%) patients with hematologic malignancies experienced HBV reactivation. Genotype D1 was detected in all five patients. Four types of mutant strains were detected in the S gene product of HBV strains and were isolated from 3 patients with HBV reactivation: T/S120, L143, and I126. HBV DNA was detected in the pretreatment HBsAg-negative samples in one of the five patients with HBV reactivation. In this patient, sequences encompassing the HBV full genome obtained from sera before the start of chemotherapy and at the time of *de novo* HBV hepatitis were detected and it showed 100% homology. Furthermore, in the phylogenetic tree, the sequences were clustered together, thereby indicating that this patient developed reactivation from an occult HBV infection.

CONCLUSION: Past infection with HBV is a risk factor for HBV reactivation in Egypt. Mandatory anti-HBc

screening prior to chemotherapy in patients with hematological malignancies is recommended.

Key words: Hepatitis B virus; Occult infection; Reactivation; Hepatitis B surface antigen

Core tip: The study aimed to investigate characteristics of hepatitis B virus (HBV) implicated in HBV reactivation in patients with hematological malignancies receiving immunosuppressive therapy in Egypt. Fifty-three hepatitis B surface antigen (HBsAg)-negative patients treated with chemotherapy were included in the study. The incidence of HBV reactivation was 9.4% among the studied cohort, and all of the affected individuals were positive for HBsAg as well as antibodies to the hepatitis B core antigen. The present study provides further evidence via molecular evolutionary analysis of the development of HBV reactivation from an occult HBV infection. Past infection with HBV is a risk factor for HBV reactivation in Egypt. Mandatory antibodies to the core antigen screening prior to chemotherapy in patients with hematological malignancies is suggested.

Elkady A, Aboulfotuh S, Ali EM, Sayed D, Abdel-Aziz NM, Ali AM, Murakami S, Iijima S, Tanaka Y. Incidence and characteristics of HBV reactivation in hematological malignant patients in south Egypt. *World J Gastroenterol* 2013; 19(37): 6214-6220 Available from: URL: http://www.wjgnet.com/1007-9327/full/v19/i37/6214.htm DOI: http://dx.doi.org/10.3748/wjg.v19.i37.6214

INTRODUCTION

Infection with hepatitis B remains one of the major causes of acute and chronic liver disease. An estimated 350-400 million people are chronically infected with hepatitis B virus (HBV) worldwide[1].

The reactivation of hepatitis B infection has been recorded in many clinical settings: chronic HBV infection after the cessation of HBV treatment, patients with malignant disease who receive immunosuppressant or chemotherapy, patients with end stage renal failure, and patients co-infected with human immunodeficiency virus (HIV)[2-6]. Patients with resolved HBV infection are diagnosed serologically by clearance of serum hepatitis B surface antigen (HBsAg) and the appearance of the hepatitis B core antibody (anti-HBc), with or without antibodies to hepatitis B surface antigen (anti-HBs)[7]. These patients are at risk of hepatitis B reactivation due to any factor that can suppress the immune system[8,9]. *De novo* hepatitis B is of particular concern in this subset of patients because it commonly leads to severe liver dysfunction and fatal hepatitis[10,11].

Occult hepatitis B is defined by the presence of HBV DNA in the serum or the liver in the absence of HBsAg, with or without anti-HBc or anti-HBs. In these patients, a low level of HBV replication has been shown to persist in the liver and in peripheral blood mononuclear cells for decades[12]. Occult HBV infection is observed worldwide, and its prevalence is related closely to the endemicity of HBV infection.

Large scale geographic heterogeneity in the prevalence of HBV had been reported worldwide. Africa is one of the highly endemic regions of HBV, and an intermediate endemicity of HBV infection had been recorded in Egypt[13,14].

The aim of this study was to investigate the incidence of HBV reactivation and the underlying risk factors of hepatitis B reactivation in Egyptian patients who received cytotoxic chemotherapy for hematological malignancies.

MATERIALS AND METHODS

Patients

Fifty-nine consecutive patients with hematological malignancies were admitted to the oncology department of Sohag Faculty of Medicine and South Egypt Cancer Institution from November 2010 to October 2011. After admission, all patients underwent physical examination and blood and serum biochemistry analyses. All of patients received chest computed tomography and ultrasonography of the abdomen as an initial evaluation.

In clinical practice, patients are monitored during chemotherapy using liver function tests. HBsAg and HBV DNA are tested in patients with elevated liver enzymes. For the purpose of this study, serum samples were collected before and after the start of the chemotherapy course. The collected sera were stored at -80 ℃ for future examination of HBsAg, anti-HBs, and anti-HBc. HBV reactivation was diagnosed when the HBsAg status changed from negative to positive after the initiation of chemotherapy and/or when HBV DNA was detected as measured by real-time detection polymerase chain reaction (RTD-PCR) using stored samples from patients, as described latter.

Serological markers of HBV infection

HBsAg was measured by enzyme immunoassay (EIA) (AxSYM; Abbott Japan, Tokyo, Japan) or chemiluminescence enzyme immunoassay (CLEIA) (Fujirebio, Tokyo; Japan). Anti-HBc of the IgG class was determined by radioimmunoassay (Abbott Japan). All serologic assays were performed according to the manufacturer's instructions.

Detection and quantitation of serum HBV DNA

HBV-DNA sequences spanning the S gene were amplified by RTD-PCR according to the previously described protocol with a slight modification and a detection limit of 100 copies/mL (equivalent to 20 IU/mL)[15].

Sequencing and molecular evolutionary analysis of HBV

Nucleic acids were extracted from serum samples (200 μL) using the QIAamp DNA extraction kit (Qiagen, Hilden,

Table 1 Characteristics of 53 patients with malignant hematologic disease who were negative for hepatitis B surface antigen *n* (%)

Characteristics	Total (n = 53)	Anti-HBc positive (n = 18)	Anti-HBc negative (n = 35)	*P* value
Age yr, mean ± SD	27.8 ± 26.2	34.4 ± 27.9	27.7 ± 25.4	0.42
Gender (male)	26 (49.1)	10 (55.6)	16 (45.7)	0.56
Diagnosis				
Malignant lymphoma	26 (40.1)	9 (50.0)	17 (48.6)	1.00
Acute leukemia	25 (47.2)	9 (50.0)	15 (42.9)	0.77
Chronic leukemia	1 (1.9)	0 (0.0)	1 (2.9)	1.00
Multiple myeloma	1 (1.9)	0 (0.0)	1 (2.9)	1.00

Anti-HBc: Antibody to hepatitis B core antigen.

Germany).

Extracted DNA was subjected to PCR for amplifying the complete genome and the specific genomic sequences bearing enhancer II /core promoter/pre-core/core regions (nt 1628-2364), as described previously[16].

Amplicons were sequenced directly using the ABI Prism Big Dye ver. 3.1 kit in the AMI 3100 DNA automated sequencer (Applied Biosystems; Foster City, CA, United States).

All sequences were analyzed in both the forward and reverse directions. HBV genotypes were determined by molecular evolutionary analysis. Reference HBV sequences were retrieved from the DDBJ/EMBL/GenBank database and aligned by CLUSTALX, and genetic distances were estimated with the 6-parameter method in the Hepatitis Virus Database (http://s2as02.genes.nig.ac.jp/)[17]. Based on the obtained distances, phylogenetic trees were constructed by the neighbor-joining (NJ) method with the mid-point rooting option. To confirm the reliability of the phylogenetic trees, bootstrap resampling tests were performed 1000 times for analysis by the ODEN program of the National Institute of Genetics.

Ethical consideration

This study was conducted in accordance with the guidelines of the Declaration of Helsinki and its subsequent amendments, and informed consent was obtained from all patients.

Statistical analysis

Statistical analysis was performed with the Fisher's exact probability test and the independent *t* test for the continuous variables using the SPSS software package (SPSS, Chicago, IL, United States). *P* values (two-tailed) less than 0.05 were considered statistically significant.

RESULTS

Patient characteristics

Six of the 59 patients with hematologic malignancies were found to be HBsAg positive and were excluded from the analysis. Therefore, a total of 53 HBsAg-negative patients were checked for the serological markers of infection with hepatitis B. The background general characteristics of the 53 HBsAg-negative patients are presented in Table 1. The mean age of the analyzed cohort was 27.8 ± 26.2 years old. Thirty-five (66%) of 53 HBsAg-negative patients were found to be anti-HBc-negative, and 18 (34%) patients were serologically positive for anti-HBc. The predominance of male patients was observed in both the anti-HBc-positive and -negative patient groups. Twenty-six patients (40.1%) were diagnosed with malignant lymphoma, whereas 25 patients (47.2%) were diagnosed with acute leukemia. Solitary cases of chronic leukemia and multiple myeloma were also included in the studied cohort. An insignificantly higher incidence of acute leukemia cases was observed in the anti-HBc-positive patients (9/18; 50%) compared with the anti-HBc-negative patients (15/35; 42.9%).

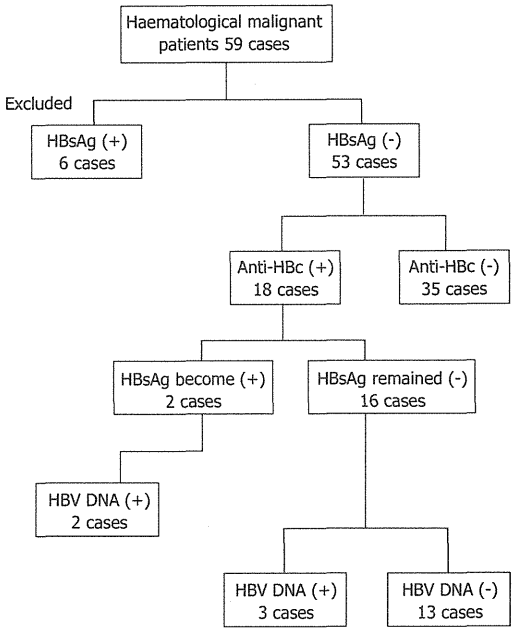

Figure 1 Longitudinal representation of hepatitis B reactivation after chemotherapy in patients with hematological malignancies. HBsAg: Hepatitis B surface antigen; anti-HBc: Antibody to hepatitis B core antigen; HBV: Hepatitis B virus.

Consequences of HBV serology after receiving anti-cancer treatment

After the initiation of systemic chemotherapy, examination of the HBV serology revealed that two (3.8%) of the HBsAg-negative patients became serologically positive for HBsAg. In addition, 3 more patients (5.8%) exhibited detectable HBV DNA in their sera after the start of the anticancer therapy (Figure 1). Interestingly, none of the serologically negative patients for anti-HBc became serologically positive for HBsAg or molecularly detectable for HBV DNA. In contrast, 2 of the 18 anti-HBc-positive patients (11.1%) became serologically positive for the HBsAg, and 3 (16.7%) became molecularly detectable for the HBV DNA. In brief, 5 of the 53 HBsAg negative

Table 2 Clinical and virological characteristics of patients who experienced hepatitis B reactivation

Characteristics	Case 1	Case 2	Case 3	Case 4	Case 5
Age (yr)/gender	79/F	8/M	11/F	5/M	20/M
Diagnosis	NHL (stage Ⅲ)	AML	ALL	ALL	ALL
Treatment[1]	CVP	St Jude protocol	St Jude protocol	St Jude protocol	St Jude protocol
HBV serology and DNA prior to chemotherapy					
HBsAg/anti-HBs/HBV DNA (log copy/mL)	(-)/(+)/1.8	(-)/(+)/negative	(-)/(-)/negative	(-)/(+)/negative	(-)/(nt)/negative
HBV reactivation months after anti-cancer therapy	12	4	5	6	4
HBV serology and DNA after chemotherapy					
HBsAg/anti-HBs/HBV DNA (log copy/mL)	(+)/(nt)/7.6	(+)/(+)/5.8	(-)/(-)/3.1	(-)/(+)/2.9	(-)/(nt)/2.0
ALT (IU/mL)	35	195	27	86	17
Total bilirubin (mg/dL)	1	1.1	1.3	1.1	0.2
Outcome	Died	Died	Died	Alive	Alive
HBV genotype	D1	D1	D1	D1	D1
Core promoter mutation	Wild	T1764/G1766	A1764	Wild	-
Pre-core A1896	Mutant	Wild	Wild	Wild	-
Amino acid mutation in S gene product	P120S/S143L	P120T	-	T126I	-

M: Male; F: Female; NHL: Non-Hodgkin lymphoma; AML: Acute myeloid leukemia; ALL: Acute lymphoblastic leukemia; HBsAg: Hepatitis B surface antigen; Anti-HBs: Antibody to hepatitis B surface antigen; CVP: Cyclophosphamide, vincristine, prednisone; ALT: Alanine amino transferase enzyme. [1]St Jude protocol: (1) prephase: vincristine + steroid; (2) induction: vincristine + farmarabin + aracytine + etoposide, intrathecal; (3) consolidation: high dose methotrexate + mercaptopurine; (4) continuation: methotrexate + mercaptopurine.

patients (9.4%), representing 27.8% (5/18) of the anti-HBc-positive patients in the studied cohort, manifested the criteria of HBV reactivation (Figure 1).

Clinical and virological criteria of the patients who manifested HBV reactivation

Five of the 53 patients (9.4%) treated for hematologic malignancies manifested HBV reactivation throughout the anti-cancer therapy regimen. The demographic, clinical and virological criteria of the HBV infection of the five patients who experienced HBV reactivation are summarized in Table 2 (cases 1-5). The mean age of the five patients was 24.6 ± 30.9 years old. Three of the patients were males (cases 2, 4 and 5), and two were females. Four patients were diagnosed with acute leukemia (cases 2-5), and only one patient (case 1) was diagnosed with malignant lymphoma. All of the 5 patients received a steroid regimen as a part of their anticancer therapy. All 5 patients were positive for anti-HBc. Three patients were positive for anti-HBs (cases 1, 2 and 4), and only one patient was serologically negative for the anti-HBs (case 3). Because of small volume of serum sample obtained from case 5, anti-HBs could not be tested. After HBV reactivation, two cases (cases 2 and 4) exhibited abnormal ALT levels, and one patient (case 2) experienced a more than 3-fold increase in the ALT level, indicating the emergence of hepatitis in this patient. None of the 5 cases who experienced had the HBV reactivation after cancer chemotherapy received an antiviral treatment for HBV.

The virological and molecular criteria are summarized in Table 2. The infecting genotype of the HBV strains was HBV genotype D, subtype D1 in all five cases. Two core promoter HBV variants were detected in 2 patients. The two variants were T1764/G1766 and A1764 in cases 2 and 3, respectively. The stop codon pre-core HBV mutant (A1896) was detected in one patient (case 1).

Infection with HBV mutant strains in the S gene product was detected in 3 patients. The amino acid escape mutant strains are as follows: S120 and L143 (case 1), T120 (case 2) and I126 (case 4). Four types of mutant strains (T/S120, L143, and I126) were detected in the S gene strains of 3 patients (cases 1, 2 and 4, respectively).

DNA sequencing and phylogenetic analysis

HBV DNA was quantified retrospectively by RTD-PCR in the stored samples of the five patients with HBV reactivation. Evidence of occult HBV infection at the time of the HBsAg-negative status (before the start of anti-cancer therapy) was detected by RTD-PCR in one patient (case 1). To determine the source of HBV infection, sera from case 1 before (case 1-A) and at the time of HBV reactivation (case 1-B) were subjected to HBV full genome amplification and sequencing. Sequences encompassing the HBV full genome obtained from sera before the start of chemotherapy and at the time of *de novo* HBV hepatitis revealed 100% homology, and the two sequences clustered together in the phylogenetic tree (Figure 2). These results demonstrate that case 1 developed reactivation from an occult HBV infection.

DISCUSSION

This study is considered the first step in documenting and characterizing the reactivation of hepatitis B in Egypt among patients negative for the HBsAg who received immunosuppressive therapy. The current study presented

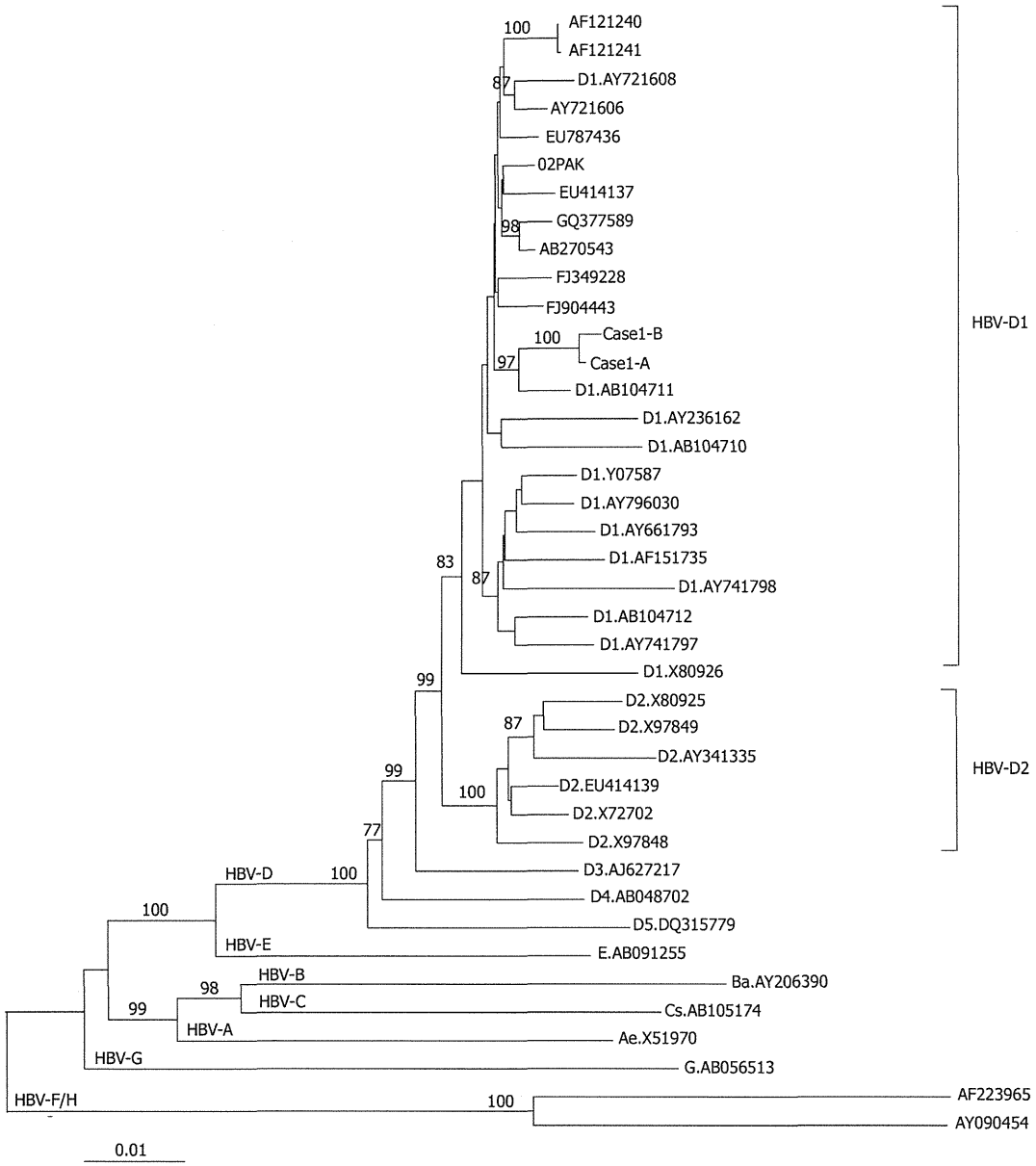

Figure 2 The complete genome of the hepatitis B virus was isolated and sequenced (case 1) prior to the start of chemotherapy (case 1-A) and after the emergence of hepatitis B virus reactivation (case 1-B). The phylogenetic analysis demonstrated that the patient (case 1) developed an hepatitis B virus (HBV) reactivation of an occult HBV infection.

further evidence that resolved hepatitis B infection and occult HBV infection may represent a hidden risk factor for the development of *de novo* hepatitis B.

The incidence of hepatitis B reactivation in the HBsAg-negative group was 9.4%, and all cases of reactivation occurred in patients with resolved or past infection with hepatitis B, as evidenced by the absence of HBsAg and the serological detection of anti-HBc. The patients who had HBV reactivation represent 27% of the HBsAg-negative/anti-HBc-positive patients. This incidence was comparable to the incidence that was described by Hui *et al*[18]. In their study, Hui *et al*[18] described an HBV reactivation incidence of 3.3% (8/244) in their studied cohort, which included HBsAg-negative lymphoma patients receiving systemic chemotherapy. Of note, all 8 patients were seropositive for either anti-HBc or anti-HBs antibody. Recently, Matsue *et al*[19] conducted a retrospective study on consecutive patients with CD20-positive B cell lymphoma before and after rituximab-containing treatment. In the latter study, 5 out of 230 patients negative for HBsAg (2.2%) experienced HBV reactivation, representing an incidence of 8.9% of the anti-HBc-positive patients[19]. In a prospective observational study of patients with hematological malignancies (a study cohort similar to the current study), Francisci *et al*[20] reported the incidence of HBV reactivation was (18%), which is close

to that detected in the present study. The reasons for the difference in the incidence in HBV reactivation among different studies remain to be elucidated. However, the intensity of treatment, patient characteristics, and geographic differences in HBV prevalence and its genotypes may account for these differences[21]. Furthermore, the lack of a clear definition of HBV reactivation should not be ignored as a possible explanation for this variation in the incidence. In this study, the inclusion of patients who had detectable HBV DNA after cancer chemotherapy plus patients who exhibited HBsAg seroconversion after receiving the anticancer therapy dramatically increased the incidence of HBV reactivation among the studied cohort. This criterion of including cases with detectable HBV DNA after cancer chemotherapy as a sign of HBV reactivation was not used to define cases with HBV reactivation in the related studies[18,19]. The variations in the cohort size among the different studies cannot be ignored as a possible factor that may be implicated in such discrepancy.

Occult HBV infection is defined by the detection of HBV DNA in the sera or in the livers of serologically HBsAg-negative patients[14]. Until recently, the clinical effects of occult HBV infection were unclear regarding the influence on the progression of liver disease, the development of hepatocellular carcinoma, the risk for HBV reactivation, and the transmission of HBV infection[22]. The underlying mechanisms for the pathogenesis of occult HBV infection may be due to either viral or host factors[23]. One of the important viral factors is the presence of mutations in the HBV DNA sequence, which may interfere with the detection of HBsAg by the commercial assays, *i.e.*, "escape mutations"[24]. In the present study, 4 types of possible escape mutants were detected in 3 of the 5 patients who experienced HBV reactivation[25]. Previous *in vitro* studies have reported that escape mutations are associated with an increased immune evasive capacity and are capable of causing symptomatic flare up and high viral loads[26]. Furthermore, studying the viral genome isolated from case 1 revealed a complete match of the sequences obtained before the start of chemotherapy and at the time of reactivation. The present study provides further evidence of the emergence of HBV reactivation of occult hepatitis B as confirmed by the molecular evolutionary analysis[27]. Furthermore, two amino acid escape mutations in the S gene product, P120S and S143L, were detected in the HBV viral genome isolated from case 1.

Patients with malignancies in Egypt are monitored only by testing ALT levels throughout the chemotherapy course. Therefore, the present study, which is the first to explore HBV reactivation in Egypt, suggests mandatory serological screening for anti-HBc and anti-HBs in patients planning to receive immunosuppressant therapy. Patients found to be positive for anti-HBc, particularly patients who are negative for anti-HBs, should be closely monitored with HBsAg, HBV DNA and serum biochemistry during chemotherapy and for at least 6 mo after the completion of therapy. Further prospective multicenter studies are needed to explore the incidence and risk factors of HBV reactivation in Egypt. Further studies are recommended to determine whether specific genomic mutations are implicated in de novo hepatitis in this subset of patients infected with HBV genotype D1.

COMMENTS

Background

The reactivation of hepatitis B is a syndrome characterized by an abrupt appearance or rise of the hepatitis B virus (HBV) DNA in the sera of patients with resolved or inactive hepatitis B infection. Reactivation can be spontaneous but is typically triggered by cancer chemotherapy, immune suppression or alterations in immune system function. Hepatitis B reactivation is of special clinical concern in immunocompromised patients because it leads to severe liver dysfunction and hepatic failure. However, hepatitis B reactivation is easy to prevent by introducing a prophylactic oral antiviral therapy. Occult hepatitis B is defined by the presence of HBV DNA in the serum or the liver in the absence of Hepatitis B surface antigen (HBsAg) with or without hepatitis B core antibody (anti-HBc) or antibodies to HBV surface antigen (anti-HBs). These patients are at risk of developing hepatitis B reactivation due to any factor suppressing the immune system. In Egypt, patients receiving cancer chemotherapy are typically monitored by liver function tests, with no screening for HBsAg or HBV DNA except in cases with elevated liver enzymes. This study aimed to investigate the incidence of HBV reactivation and the underlying risk factors of reactivation in Egyptian patients with hematological malignancies who were receiving cancer chemotherapy.

Research frontiers

In a cohort of 53 patients with hematological malignancies receiving cancer chemotherapy who were negative for HBsAg, 18 patients (34%) were found to be positive for the anti-HBc, and five of the 53 (9.4%) patients with hematologic malignancies experienced HBV reactivation. All five patients were positive for anti-HBc. HBV DNA was detected in pretreatment HBsAg-negative samples in one of the five patients with HBV reactivation. In this patient, sera were obtained before the start of chemotherapy and at the time of *de novo* HBV hepatitis; the molecular evolutionary analysis of the sequences encompassing the HBV full genome obtained from the sera revealed that this patient developed reactivation from an occult HBV infection.

Innovations and breakthroughs

This study is the first in Egypt to characterize HBV reactivation in Egypt. The study introduces more evidence through molecular evolutionary analysis that occult HBV infection is a risk factor for reactivation of hepatitis B in patients with hematological malignancies receiving cancer chemotherapy.

Applications

The study strongly recommends mandatory serological screening for anti-HBc and anti-HBs in this subset of patients before the commencement of chemotherapy. Patients found to be positive for anti-HBc, particularly patients who are negative for anti-HBs, should be closely observed for signs of HBV reactivation through the regular monitoring of HBsAg and HBV DNA.

Peer review

In the study, performance of sequencing and molecular analysis of HBV genomes seems relevant in characterization of the strains associated with HBV reactivation. Their findings are significant and beneficial for the readers.

REFERENCES

1 **Lee WM**. Hepatitis B virus infection. *N Engl J Med* 1997; **337**: 1733-1745 [PMID: 9392700 DOI: 10.1056/NEJM199712113372406]

2 **Freudiger H**, Sitavanc R. Reverse seroconversion of hepatitis B in a haemodialysis patient. *Nephrol Dial Transplant* 2004; **19**: 238-241 [PMID: 14671065 DOI: 10.1093/ndt/gfg448]

3 **Schnepf N**, Sellier P, Bendenoun M, Zini JM, Sanson-le Pors MJ, Mazeron MC. Reactivation of lamivudine-resistant occult hepatitis B in an HIV-infected patient undergoing cytotoxic chemotherapy. *J Clin Virol* 2007; **39**: 48-50 [PMID: 17368969 DOI: 10.1016/j.jcv.2007.01.011]

4 **Chakvetadze C**, Bani-Sadr F, Le Pendeven C, Lamontagne F, Vincensini JP, Pialoux G. Reactivation of hepatitis B virus

replication during peginterferon-ribavirin therapy in an HIV/hepatitis C virus-co-infected patient with isolated anti-hepatitis B core antibodies. *AIDS* 2007; **21**: 393-394 [PMID: 17255759 DOI: 10.1097/QAD.0b013e328012b5d3]

5 **Clark SJ**, Creighton S, Horner M, Smith HM, Portmann B, Taylor C, Cramp ME. Reactivation of latent hepatitis B virus infection with HIV-related immunosuppression. *Int J STD AIDS* 2006; **17**: 67-69 [PMID: 16409685 DOI: 10.1258/095646206775220612]

6 **Bortolotti F**, Crivellaro C, Brunetto MR, Cadrobbi P, Bertolini A, Alberti A. Selection of a precore mutant of hepatitis B virus and reactivation of chronic hepatitis B acquired in childhood. *J Pediatr* 1993; **123**: 583-585 [PMID: 8410512 DOI: 10.1016/S0022-3476(05)80956-4]

7 **Lowell JA**, Howard TK, White HM, Shenoy S, Huettner PC, Brennan DC, Peters MG. Serological evidence of past hepatitis B infection in liver donor and hepatitis B infection in liver allograft. *Lancet* 1995; **345**: 1084-1085 [PMID: 7715341 DOI: 10.1016/S0140-6736(95)90819-6]

8 **Nordbø SA**, Skaug K, Holter E, Waage A, Brinch L. Reactivation of hepatitis B virus infection in an anti-HBc and anti-HBs positive patient after allogeneic bone marrow transplantation. *Eur J Haematol* 2000; **65**: 86-87 [PMID: 10914949 DOI: 10.1034/j.1600-0609.2000.91228.x]

9 **Chamorro AJ**, Casado JL, Bellido D, Moreno S. Reactivation of hepatitis B in an HIV-infected patient with antibodies against hepatitis B core antigen as the only serological marker. *Eur J Clin Microbiol Infect Dis* 2005; **24**: 492-494 [PMID: 15990987 DOI: 10.1007/s10096-005-1355-1]

10 **Kitano K**, Kobayashi H, Hanamura M, Furuta K, Ueno M, Rokuhara A, Tanaka E, Umemura T, Kiyosawa K. Fulminant hepatitis after allogenic bone marrow transplantation caused by reactivation of hepatitis B virus with gene mutations in the core promotor region. *Eur J Haematol* 2006; **77**: 255-258 [PMID: 16923112 DOI: 10.1111/j.1600-0609.2006.00678.x]

11 **Lin PC**, Poh SB, Lee MY, Hsiao LT, Chen PM, Chiou TJ. Fatal fulminant hepatitis B after withdrawal of prophylactic lamivudine in hematopoietic stem cell transplantation patients. *Int J Hematol* 2005; **81**: 349-351 [PMID: 15914368 DOI: 10.1532/IJH97.A10411]

12 **Hu KQ**. Occult hepatitis B virus infection and its clinical implications. *J Viral Hepat* 2002; **9**: 243-257 [PMID: 12081601 DOI: 10.1046/j.1365-2893.2002.00344.x]

13 **Ozaslan E**, Purnak T. Controversies about occult hepatitis B virus infection. *World J Gastroenterol* 2009; **15**: 4986-4987 [PMID: 19842236 DOI: 10.3748/wjg.15.4986]

14 **Raimondo G**, Pollicino T, Cacciola I, Squadrito G. Occult hepatitis B virus infection. *J Hepatol* 2007; **46**: 160-170 [PMID: 17112622 DOI: 10.1016/j.jhep.2006.10.007]

15 **Sugiyama M**, Tanaka Y, Kurbanov F, Maruyama I, Shimada T, Takahashi S, Shirai T, Hino K, Sakaida I, Mizokami M. Direct cytopathic effects of particular hepatitis B virus genotypes in severe combined immunodeficiency transgenic with urokinase-type plasminogen activator mouse with human hepatocytes. *Gastroenterology* 2009; **136**: 652-662.e3 [PMID: 19041311 DOI: 10.1053/j.gastro.2008.10.048]

16 **Sugauchi F**, Orito E, Ichida T, Kato H, Sakugawa H, Kakumu S, Ishida T, Chutaputti A, Lai CL, Ueda R, Miyakawa Y, Mizokami M. Hepatitis B virus of genotype B with or without recombination with genotype C over the precore region plus the core gene. *J Virol* 2002; **76**: 5985-5992 [PMID: 12021331 DOI: 10.1128/JVI.76.12.5985-5992.2002]

17 **Shin-I T**, Tanaka Y, Tateno Y, Mizokami M. Development and public release of a comprehensive hepatitis virus database. *Hepatol Res* 2008; **38**: 234-243 [PMID: 17877727 DOI: 10.1111/j.1872-034X.2007.00262.x]

18 **Hui CK**, Cheung WW, Zhang HY, Au WY, Yueng YH, Leung AY, Leung N, Luk JM, Lie AK, Kwong YL, Liang R, Lau GK. Kinetics and risk of de novo hepatitis B infection in HBsAg-negative patients undergoing cytotoxic chemotherapy. *Gastroenterology* 2006; **131**: 59-68 [PMID: 16831590 DOI: 10.1053/j.gastro.2006.04.015]

19 **Matsue K**, Kimura S, Takanashi Y, Iwama K, Fujiwara H, Yamakura M, Takeuchi M. Reactivation of hepatitis B virus after rituximab-containing treatment in patients with CD20-positive B-cell lymphoma. *Cancer* 2010; **116**: 4769-4776 [PMID: 20597091 DOI: 10.1002/cncr.25253]

20 **Francisci D**, Falcinelli F, Schiaroli E, Capponi M, Belfiori B, Cecchini E, Baldelli F. Reactivation of hepatitis B virus replication due to cytotoxic therapy: a five-year prospective study. *Tumori* 2012; **98**: 220-224 [PMID: 22677988]

21 **Chu CM**, Liaw YF. Genotype C hepatitis B virus infection is associated with a higher risk of reactivation of hepatitis B and progression to cirrhosis than genotype B: a longitudinal study of hepatitis B e antigen-positive patients with normal aminotransferase levels at baseline. *J Hepatol* 2005; **43**: 411-417 [PMID: 16006001 DOI: 10.1016/j.jhep.2005.03.018]

22 **Romero M**, Madejón A, Fernández-Rodríguez C, García-Samaniego J. Clinical significance of occult hepatitis B virus infection. *World J Gastroenterol* 2011; **17**: 1549-1552 [PMID: 21472119 DOI: 10.3748/wjg.v17.i12.1549]

23 **Said ZN**. An overview of occult hepatitis B virus infection. *World J Gastroenterol* 2011; **17**: 1927-1938 [PMID: 21528070 DOI: 10.3748/wjg.v17.i15.1927]

24 **Samal J**, Kandpal M, Vivekanandan P. Molecular mechanisms underlying occult hepatitis B virus infection. *Clin Microbiol Rev* 2012; **25**: 142-163 [PMID: 22232374 DOI: 10.1128/CMR.00018-11]

25 **Zaaijer HL**, Torres P, Ontañón A, Ponte LG, Koppelman MH, Lelie PN, Hemert FJ, Boot HJ. Multiple surface antigen mutations in five blood donors with occult hepatitis B virus infection. *J Med Virol* 2008; **80**: 1344-1349 [PMID: 18551607 DOI: 10.1002/jmv.21233]

26 **Henke-Gendo C**, Amini-Bavil-Olyaee S, Challapalli D, Trautwein C, Deppe H, Schulz TF, Heim A, Tacke F. Symptomatic hepatitis B virus (HBV) reactivation despite reduced viral fitness is associated with HBV test and immune escape mutations in an HIV-coinfected patient. *J Infect Dis* 2008; **198**: 1620-1624 [PMID: 18847320 DOI: 10.1086/592987]

27 **Sugauchi F**, Tanaka Y, Kusumoto S, Matsuura K, Sugiyama M, Kurbanov F, Ueda R, Mizokami M. Virological and clinical characteristics on reactivation of occult hepatitis B in patients with hematological malignancy. *J Med Virol* 2011; **83**: 412-418 [PMID: 21264861 DOI: 10.1002/jmv.21995]

P- Reviewers Jang JW, Suzukawa K, Zhou YH
S- Editor Wen LL **L- Editor** A **E- Editor** Zhang DN

Journal of Controlled Release 173 (2014) 110–118

Contents lists available at ScienceDirect

Journal of Controlled Release

journal homepage: www.elsevier.com/locate/jconrel

RNAi-mediated gene knockdown and anti-angiogenic therapy of RCCs using a cyclic RGD-modified liposomal-siRNA system

Yu Sakurai [a], Hiroto Hatakeyama [a], Yusuke Sato [a], Mamoru Hyodo [a], Hidetaka Akita [a], Noritaka Ohga [b], Kyoko Hida [b], Hideyoshi Harashima [a,*]

[a] Laboratory of Innovative Nanomedicine, Faculty of Pharmaceutical Sciences, Hokkaido University, Kita 12, Nishi 6, Kita-ku, Sapporo 060-0812, Japan
[b] Division of Vascular Biology, Graduate School of Dental Medicine, Hokkaido University, Kita 13 Nishi 7, Kita-ku, Sapporo 060-0812, Japan

ARTICLE INFO

Article history:
Received 21 May 2013
Accepted 3 October 2013
Available online 11 October 2013

Keywords:
siRNA
Liposome
Anti-angiogenic therapy
Cyclic RGD
Active targeting

ABSTRACT

Angiogenesis is one of crucial processes associated with tumor growth and development, and consequently a prime target for cancer therapy. Although tumor endothelial cells (TECs) play a key role in pathological angiogenesis, investigating phenotypical changes in neovessels when a gene expression in TEC is suppressed is a difficult task. Small interfering RNA (siRNA) represents a potential agent due to its ability to silence a gene of interest. We previously developed a system for *in vivo* siRNA delivery to cancer cells that involves a liposomal-delivery system, a MEND that contains a unique pH-sensitive cationic lipid, YSK05 (YSK-MEND). In the present study, we report on the development of a system that permits the delivery of siRNA to TECs by combining the YSK-MEND and a ligand that is specific to TECs. Cyclo(Arg-Gly-Asp-D-Phe-Lys) (cRGD) is a well-known ligand to $\alpha_V\beta_3$ integrin, which is selectively expressed at high levels in TECs. We incorporated cRGD into the YSK-MEND (RGD-MEND) to achieve an efficient gene silencing in TECs. Quantitative RT-PCR and the 5′ rapid amplification of cDNA ends PCR indicated that the intravenous injection of RGD-MEND at a dose of 4.0 mg/kg induced a significant RNAi-mediated gene reduction in TEC but not in endothelial cells of other organs. Finally, we evaluated the therapeutic potency of the RGD-MEND encapsulating siRNA against vascular endothelial growth factor receptor 2. A substantial delay in tumor growth was observed after three sequential RGD-MEND injections on alternate days. In conclusion, the RGD-MEND represents a new approach for the characterization of TECs and for us in anti-angiogenic therapy.

1. Introduction

Angiogenesis is a major cause in cancer progression and metastasis [1,2]. Folkman et al. first proposed the theory that, to be supplied with oxygen and other nutrients, tumors with sizes over 1–2 mm^3 inevitably required angiogenesis, and that, if tumor vasculature development could be inhibited, tumor tissue would shrink, as the result of a lack of oxygen and other nutrients [3]. Since this publication, anti-angiogenic therapy has evolved as an innovative treatment for various cancers. A mono-clonal antibody against vascular endothelial growth factor (VEGF), which is referred to as Avastin, is currently used in the treatment of various types of cancer [4,5].

Small interfering RNA (siRNA) was predicted to be a potentially useful drug for this purpose, due to the ability to inhibit the expression of any genes of interest in a sequence-specific manner [6]. However, its instability in the blood and the low permeability of the plasma membrane require drug delivery systems that target specific cells in order to achieve an effective therapy by siRNA [6,7]. We previously developed a liposomal siRNA system, a multi functional nano-device (MEND) [8,9]. In the past report, the use of a MEND composed of a pH-sensitive cationic lipid, YSK05 (YSK-MEND) caused a significant gene reduction in tumor tissue when intratumorally and intravenously injected into tumor-bearing mice [10,11]. A number of pH sensitive siRNA carriers, such as liposomes [12,13], polyplexes [14] and micelles [15], have been evaluated for use in tumor targeting. pH-sensitive carriers are generally thought to be more suitable for tumor targeting than conventional cationic carriers because of their highly specific fusiogenicity in acidic endosomes [16]. YSK05 consists of two linoleyl fatty acid chains and a tertiary amino group, which are responsible for pH-responsive fusiogenicity in endosomes. In this study, we incorporated a ligand that is specific to tumor endothelial cells (TECs) into YSK-MEND to achieve anti-angiogenic therapy using siRNA.

Cyclo (Arg-Gly-Asp-D-Phe-Lys) (cRGD) peptide is a well-validated ligand for $\alpha_V\beta_3$ integrin, which is highly and selectively expressed on the cell surface of TECs and some types of cancer cells themselves [17]. cRGD is a known antagonist of $\alpha_V\beta_3$ integrin, and the injection of free cRGD suppresses tumor progression in many cancers such as glioblastomas and lung cancer [18]. This is because $\alpha_V\beta_3$ integrin plays a key role in angiogenesis in tumor tissue [19]. Moreover, the cRGD peptide can be

* Corresponding author at: Kita-12, Nishi-6, Kita-ku, Sapporo 060-0812, Japan. Tel.: +81 11 706 3919; fax: +81 11 706 4879.
E-mail address: harasima@pharm.hokudai.ac.jp (H. Harashima).

0168-3659/$ – see front matter © 2013 Elsevier B.V. All rights reserved.
http://dx.doi.org/10.1016/j.jconrel.2013.10.003

used for a variety of purposes, including cancer imaging and therapy by conjugating cRGD with imaging probes, anti-cancer agents or drug carriers [20]. Concerning the *in vivo* delivery of nucleic acids using cRGD, several reports have appeared in which tumor growth was inhibited by the systemic injection of anti-tumor and/or anti-angiogenic oligonucleotides encapsulated in micelles [21] and lipoplexes [22–24]. However, in almost all of those reports it was not clear whether siRNA was delivered to cancer cells and TECs, and no direct evidence showing that a gene reduction in TECs was mediated by RNA interference. In this study, we verified gene silencing by siRNA in TECs using quantitative RT-PCR (qRT-PCR) and rapid amplification of the 5′ cDNA ends (5′ RACE-PCR), which was the only method available for confirming RNAi-induced silencing [7].

We chose renal cell carcinomas (RCCs) as a therapeutic model cancer by inhibiting angiogenesis, since it is well known that RCCs effectively respond to anti-angiogenic therapy [25]. Since RCCs are known to respond poorly to conventional anti-cancer drugs, interleukin-2 and interferon-α injections are currently the standard treatment for patients with progressive RCCs [26]. In recent years, however, novel agents targeting angiogenesis pathways have been developed as the result in advances in our understanding of tumor biology. Actually, Afinitor and Toricel (mTOR inhibitors) and Sutent (a multi kinase inhibitor) are currently being applied for metastatic RCCs in addition to Avastin.

Although anti-angiogenic treatment has had significant therapeutic effects for cancer progress and metastasis, it has been reported that some patients are refractory or acquire resistance to VEGF inhibition [27]. Several mechanisms are thought to be involved in the resistance anti-angiogenic treatment by VEGF blockade. Compensation by other pro-angiogenic mechanisms, such as basic fibloblast growth factors (bFGF), platelet-derived growth factor (PDGF) and angiopoietins, appears to be a dominant factor in the development of acquired resistance to VEGF inhibition. Moreover, recent reports suggest that the recruitment of other cells, such as pericytes and bone marrow-derived myeloid cells, to tumor vessels is implicated in the resistance to anti-angiogenic therapy [28,29]. A methodology that will permit the complete control any gene that is expressed in TECs is needed for further elucidating the mechanism of anti-angiogenic therapy resistance, and hence developing a better therapy that targets tumor angiogenesis. In the study, we report that the RGD-MEND represents an efficient siRNA delivery system for cancer treatment through anti-angiogenic therapy.

2. Materials and methods

2.1. Materials

1,2-Distearoyl-sn-glycerophosphocholine (DSPC), 1-palmitoyl-2-oleoyl-sn-glycerophosphoethanolamine (POPE), 1,2-dimyristoyl-sn-glycerol, methoxypolyethylene $glycol_{2000}$ (PEG-DMG), 1,2-distearoyl-sn-glycerol, methoxypolyethylene $glycol_{2000}$ (PEG-DSG) and N-hydroxysuccinimide-polyethylene $glycol_{2000}$-1,2-disteaoyl-sn-glycerophosphoethanolamine (NHS-PEG-DSPE) were purchased NOF (Tokyo, Japan). Cholesterol (chol), RPMI-1640 medium and DMEM were obtained from SIGMA Aldrich (St. Louis, MO). Egg phosphatidyl choline (EPC) and 1,2-distearoyl-sn-grycelo, methoxy polyethylene glycol (PEG-DSPE) were purchased from Avanti Polar Lipids (Alabaster, AL). siRNAs were obtained from Hokkaido System Science Co., Ltd. (Sapporo, Japan). [^{3}H]-choresteryl hexadecyl ether (CHE) was purchased from PerkinElmer Life Science (Tokyo, Japan). DiI and DiD were purchased from Invitrogen (Carlsbad, CA).

2.2. Synthesis of cRGD conjugates

We synthesized cRGD-conjugated PEG (RGD-PEG) as previously reported [30]. In brief, cRGD peptide was incubated with NHS-PEG-DSPE in 20 mM phosphate buffered saline (pH 7.4, PBS) at 37 °C for 12 h. The mixture was then subject to dialysis using Spectra Por 6 (MWCO 1000 Da, Spectrum) to remove un-conjugated RGD. The molecular weight of the conjugate was determined by MALDI TOF-MS.

2.3. MEND preparation

YSK-MENDs were prepared as previously reported [10,11]. Briefly, 1500 nmol of YSK05, 750 nmol of POPE, 750 nmol chol and 150 nmol PEG-DMG were dissolved in 400 μL of 90% (v/v) aqueous tertiary butanol (t-BuOH). When the fluorescence was incorporated into the YSK-MENDs, 0.5 mol% (of the total lipid) DiD was added to the tubes and the organic solvent was removed by evaporation before the lipid solution was mixed. Two hundred microliters of siRNA solution (concentration 0.8 mg/mL in 2 mM filter-sterilized citrate buffer (pH4.5)) was gradually added to the shaking lipid solution, and homogenous particles of liposomal siRNA were spontaneously formed by drastically diluting the siRNA–lipid mixture to 2 mL with 20 mM citrate buffer. The t-BuOH was then removed by ultrafiltration. For RGD-modification, a RGD–PEG solution was incubated with a YSK-MEND solution at 60 °C for 30 min at various molar ratios (RGD-PEG/total lipid of YSK-MEND). The YSK-MENDs were characterized by a Zetasizer Nano ZS ZEN3600 instrument (Malvern Instruments, Worchestershire, UK). The encapsulation efficiency and recovery ratio were calculated using RiboGreen (Invitrogen) as previously described [10]. siRNA encapsulation efficiency rate of all MENDs used in this study was over 90%. The sequences of the used siRNAs are shown in Supplemental Table S1.

2.4. Cell culture

OS-RC-2 cells and HEK293T cells were cultured in RPMI-1640 and DMEM, respectively. These media were supplemented with 10% fetal bovine serum, penicillin (100 U/mL) and streptomycin (100 μg/mL). TECs, which were previously isolated by Ohga et al. [31], and HUVEC were cultured in EBM-2 medium supplemented with 2% FBS (v/v) and bullet kits (Lonza, Walkersville, MD). All cells were maintained at 37 °C in a 5% CO_2 humidified atmosphere.

2.5. Evaluation of antigen expression

For evaluating the expression of $\alpha_V\beta_3$ integrin, 1.0×10^6 trypsinized cells were suspended in 1 mL of FACS buffer (0.5% bovine serum albumin and 0.1% sodium azide in 20 mM PBS), and the suspension was centrifuged at 4 °C for 4 min at 500 ×*g*. The cells were incubated in 100-fold diluted anti human $\alpha_V\beta_3$ integrin rat IgG (R&D systems, Minneapolis, MN) for 30 min on ice. The antibody solution was then removed by centrifugation and the cells were washed twice with 500 μL of FACS buffer. Two hundred-fold diluted Alexa633-labeled anti rat IgG goat F(ab′) (Invitrogen) was added to the cells. The cells were washed twice with 500 μL of FACS buffer, and re-suspended in 1 mL of FACS buffer. The cell suspension was analyzed by FACSCalibur (Becton Dickinson, Franklin Lakes, NJ).

2.6. Animal study

Male, 4-week-old ICR mice and BALB/cAJcl-*nu/nu* were purchased from Japan SLC (Shizuoka, Japan) and CLEA (Tokyo, Japan), respectively. For preparing OS-RC-2-bearing mice, 1.0×10^6 OS-RC-2 cells in 75 μL of sterilized PBS were inoculated into anesthetized BALB/cAJcl-*nu/nu* mice on the right flank. The experimental protocols were reviewed and approved by the Hokkaido University Animal Care Committee in accordance with the Guide for the Care and Use of Laboratory Animals.

2.7. Confocal laser scanning microscopy (CLSM) to determine the localization in tumor tissue of the MEND

OS-RC-2-bearing mice were intravenously administered with 3.0 mg/kg of DiD labeled-YSK-MEND. FITC-labeled Isolectin B4 (Vector Laboratories, Burlingame, CA) were injected via the tail vein 10 min before collecting. Tumor tissue was excised 24 h after injection of the YSK-MENDs, and then fixed with 4% paraformaldehyde (PFA). Fixed tumor tissue was washed with 10%, 30% and 50% sucrose over night. Tumor tissue was embedded in OCT compound, and 16 μm thick slices were prepared on the slideglass SUPERFROST S9441 (MATUSNAMI) with CM-3050S (Leica, Wetzlar, Germany). Tumor slices were washed with PBS twice, and covered with a cover glass. The tumor slices were observed with an FV10i-LIV microscope.

2.8. Flowcytometry (FCM) analysis for the internalization of MEND into cells

To investigate the localization of the YSK-MENDs in tumor tissue after systemic injection, OS-RC-2 bearing mice were systemically injected with DiD labeled-YSK-MENDs at a dose of 3 mg/kg. Tumor tissue was collected 6 h after injection, and then shredded. The shredded tumor tissue was then incubated in 2 mL of Hanks' Balanced Salt Solution (HBSS, SIGMA Aldrich) containing 20 mg of type I collagenase (Gibco, Rockville, MD), 200 μg of DNase I (Gibco), 1 mL of inactivated FBS and 2.0 mmol of $CaCl_2$ for 30 min at 37 °C. The resulting cell suspension was filtered through a 100 μm Cell Strainer (BD Falcon), and then centrifuged at 4 °C for 3 min at 500 rpm after the addition of 10 mL of HBSS and the supernatant was removed. This "washing procedure" was repeated 2 times. To remove red blood cells, the centrifuged cells were incubated in Red Blood Cell Lysing Buffer (SIGMA Aldrich) for a several minutes at room temperature and the washing procedure was repeated once. Next, 1.0×10^6 cells were incubated with an anti mouse PE-labeled CD31 antibody (Biolegend, San Diego, CA) or PE-labeled Rat IgG2a, κ isotype control (Biolegend) for 30 min on ice. Cells were washed, and then analyzed with FACSCalibur 10 min after 7-AAD (IMGENEX, San Diego, CA) addition. The 7-AAD-positive population was assumed to be dead cells and were gated out.

2.9. Evaluation for gene silencing by qRT-PCR

Cells plated onto 6-well plate were lysed by treatment with 350 μL of TRIzol (Invitrogen). For the *in vivo* experiment, approximately 50 mg of collected tissue was homogenized by means of a PreCellys (Bertin Technologies, Montigny-Le-Bretonneux, France) in 500 μL of TRIzol, and then centrifuged at 12,000 ×*g* at 4 °C for 15 min. Supernatant was used as an RNA extraction sample. RNA extraction and purification was then performed according to the manufacturers' protocol. One microgram of total RNA was subjected to reverse transcription reaction using a High Capacity RNA-to-cDNA kit (Applied Biosystems, Foster City, CA).

Fifty-fold diluted cDNA was subject to qPCR with Fast SYBR Green Master Mix (Applied Biosystems) using LightCycler-480 (Roche Diagnostics, Germany). The reaction conditions were according to the manufacturer's protocol. The sequences of all primer sets in the experiment are shown in Supplemental Table S1.

2.10. Confirmation of RNAi-mediated gene silencing by 5′ RACE-PCR

5′ RACE-PCR for the detection of *Cd31* mRNA cleaved by si-*Cd31* was carried out as previously reported [11]. Briefly, GeneRacer Adaptor was ligated into cleaved *Cd31* mRNA, and then reverse transcribed with *Cd31* Gene Specific Primer by SuperScript III (Invitrogen). Next, cDNA was amplified by 2 times PCR (i.e. nested PCR) with 2 different sets of PCR primers (Ad5 outer and *Cd31* outer primers for the 1st PCR, and Ad5 inner and *Cd31* inner primers for the 2nd PCR). All oligonucleotides used in the procedure are shown in Supplemental Table S1.

2.11. Somatic and hepatic toxicity

Liver toxicity was evaluated 24 h after injection of the MEND at a dose of 3.0 mg/kg. Serum asparate aminotransferase (AST) and alanine aminotransferase (ALT) were measured using a transaminase CII test kit (Wako Pure Chemicals, Osaka, Japan) in accordance with manufacturer's instructions.

2.12. Statistical analysis

Comparisons between multiple treatments were made using one-way ANOVA, followed by the Bonferroni test. Pair-wise comparisons between treatments were made using a Student's *t*-test. A p-value of <0.05 was considered significant.

3. Results

3.1. Preparation and characterization of YSK-MEND modified with RGD-PEG (RGD-MEND)

The expression of integrin $\alpha_V\beta_3$ in two cell lines was determined by FCM (Fig. 1).

We next evaluated the optimal modification ratio of RGD-PEG into the YSK-MEND at 0–10 mol% against the total lipid. The lipid composition of the YSK-MEND was YSK05/POPE/chol/PEG-DMG (50/25/25/3, molar ratio), which showed the most efficient silencing effect in the *in vitro* cultured cell line [10]. The PEG-DSPE (without cRGD) modified YSK-MEND (PEG-MEND) was regarded as a negative control in the *in vitro* study. The characteristics of these RGD-MENDs are shown in Table 1. In HUVEC, a 5.0 mol% modification facilitated the cellular internalization of the YSK-MEND to the greatest extent (Fig. 2). However, a further increase was not observed when the modification ratio was 10 mol% against the total lipid. On the other hand, no change in the cellular uptake of nanoparticles was observed in the case of HEK293T cells. We also carried out this cellular uptake experiment with RGD-modified liposomes (Fig. S1), and similar results were observed in FCM and CLSM studies. Taken together, we conclude that the RGD-incorporation ratio was 5.0 mol%. In addition, RGD-modification had no effect on the pH-sensitivity of the YSK-MEND (Fig. S2). Next, we evaluated the knockdown effect of RGD-MEND. Anti polo-like kinase 1 siRNA (si-*PLK1*) formulated into both RGD-MEND and PEG-MEND was added to HUVEC and HEK293T at a concentration of 11–100 nM. Anti-luciferase siRNA (si-*luc*) was used as a negative control siRNA. The

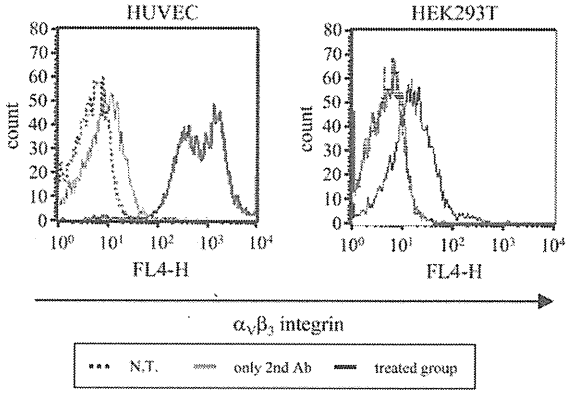

Fig. 1. $\alpha_V\beta_3$ integrin expression in HUVEC and HEK293T cells. HUVEC (left panel) and HEK293T (right panel) were treated with anti-$\alpha_V\beta_3$ integrin antibody and s fluorescence labeled-2nd antibody, and then analyzed by FCM. In the histograms, the black dotted line, the black solid line and the gray solid line denote untreated cells, cells treated with both the 1st and 2nd antibody and cells treated with only the 2nd antibody, respectively. N.T.: non treatment.

Table 1
Characteristics of the RGD-MENDs used in the *in vitro* cellular uptake experiments.

	RGD-modified MEND				
Lipid composition	YSK05/POPE/chol/PEG-DMG 50/25/25/3				
RGD-PEG (mol%)	0	1.0	2.5	5.0	10
Diameter (nm)	106 ± 6	107 ± 8	106 ± 10	101 ± 3	110 ± 12
PdI	0.10 ± 0.02	0.15 ± 0.01	0.16 ± 0.04	0.13 ± 0.02	0.22 ± 0.05
ζ-potential (mV)	−5 ± 3	−6 ± 5	−9 ± 10	−11 ± 4	−13 ± 8

Data represents mean ± SD.

RGD-MEND reduced target gene expression in a dose-dependent manner, while the PEG-MEND caused no detectable changes in target gene expression in HUVEC (Fig. 3A). In the case of HEK293T, however, neither the PEG-MEND nor the RGD-MEND induced gene silencing (Fig. 3B). On the other hand, si-*PLK1* transfection with RNAiMAX significantly inhibited *PLK1* expression in HEK293T cells (Fig. S3). This result clearly shows that HEK293T was not refractory to si-*PLK1*.

3.2. Localization of RGD-MEND after systemically injection

We next investigated the tumor accumulation of RGD-MEND intravenously injected into mice. Tumor distribution was observed by CLSM and FCM in order to detect the specific delivery siRNA to TECs, not tumor whole tissue. To evaluate the targeting potency of the RGD-MEND, we compared with active targeting RGD-MEND with a "cancer cell targeting" YSK-MEND (a conventional YSK-MEND), which was originally developed for silencing cancer cell genes [11]. Generally speaking, liposomes with a prolonged circulation time after systemic injection can passively accumulate and diffuse in tumor tissue through the enhanced permeability and retention (EPR) effect [32]. The EPR effect is caused by increasing vessel permeability and decreasing lymphatic drainage in tumor tissue due to the development of an aberrant tumor vasculature. The conventional YSK-MEND could circulate in blood stream as previously shown [11], and consequently accumulated and spread in tumor tissue. Therefore, the non-active targeting conventional YSK-MEND achieved "cancer cell targeting" via the EPR effect, which resulted in a significant gene silencing in cancer cells. In addition, we previously reported that non-ligand PEG-MEND (YSK05/POPE/chol/PEG-DMG 50/25/25/3) was not able to deliver siRNA in target organs, and concluded that the PEG-MEND could not be used as a negative control in the *in vivo* study. Taken together, in the *in vivo* section, the conventional YSK-MEND was regarded as a control non-TEC targeting carrier. The characteristics and lipid composition of the MENDs used in the *in vivo* experiments are shown in Table 2. Actually we were not able to observe the effective knockdown in TECs after the injection of the conventional YSK-MEND (Fig. S4). In TECs, the DiD signal was detected only in the group treated with the RGD-MEND (Fig. 4A). In addition, the RGD-MEMD was co-localized with TECs (Figs. 4B, S5). However, the intravenously injected conventional YSK-MEND was not observed in TECs but was diffused over the entire tumor tissue. To demonstrate the effect of cRGD, we also investigated the targeting ability and the knockdown efficiency of the PEG-MEND (YSK-MEND modified with PEG-DSPE instead of RGD-PEG). The systemically injected PEG-MEND neither accumulated in TECs (Fig. S6A) nor inhibited TECs-specific gene expression (Fig. S6B).

Regarding the distribution in other organs, a high accumulation of systemically administered RGD-MEND was detected in the liver, spleen and lungs (Fig. S7).

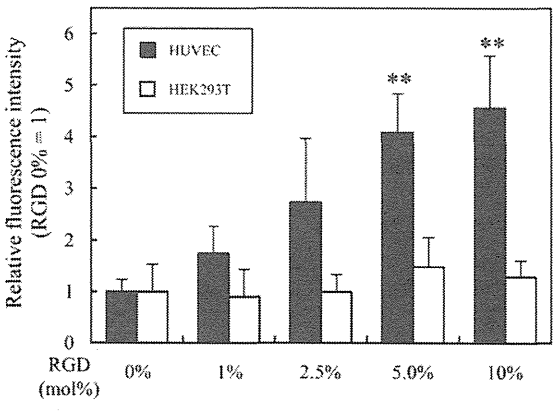

Fig. 2. Cellular uptake of RGD-MENDs containing various amounts of RGD-PEG. Cellular uptake was determined by FCM at 3 h after adding the fluorescence-labeled MENDs to the cells. In the graph, the fluorescence intensity was normalized to RGD 0% in each cell line. White columns and black columns indicate the cellular uptake of HUVEC and that of HEK293T, respectively. **: $p < 0.01$ (ANOVA followed by Bonferroni correction vs. RGD 0% in HUVEC. $n = 3$).

3.3. Selective gene silencing of systemic administered RGD-MEND

We then evaluated the *in vivo* knockdown and therapeutic effect of the RGD-MEND. To specifically determine the extent of gene knockdown in TECs, *Cd31*, which is selectively expressed in both TECs and normal endothelial cells (ECs), was used. OS-RC-2-bearing mice were treated with anti *Cd31* siRNA (si-*Cd31*) encapsulated in the RGD-MEND at a dose ranging from 0.5 to 4.0 mg/kg. As a result, the RGD-MEND caused a reduction in *Cd31* expression in a dose-dependent manner while the si-*luc* encapsulated in RGD-MEND did not (Fig. 5A). In contrast, RGD-MEND did not downregulate the gene in cancer cells (Fig. S8). Furthermore, we confirmed that this inhibition was caused by RNAi with 5′ RACE-PCR (Fig. 5B). As a result of a 5′ RACE-PCR experiment, approximately 250 bp of PCR products were obtained at a dose of 4.0 mg/kg. Thus, the reduction in *Cd31* expression can be attributed to an RNAi-mediated mechanism (Fig. 5C). To evaluate the possibility that RGD-MEND injection causes side effects, we investigated the silencing effect of other organs' ECs. However, no inhibitory effect on the siRNA-target gene was observed in these tissues (Fig. S9).

3.4. Therapeutic effect of si-Vegfr2 encapsulated in the RGD-MEND

Finally, we examined the therapeutic effect of the RGD-MEND. *VEGFR2* is one of the dominant factors in angiogenesis, and the inhibition of VEGFR2 by an antibody induced anti-tumor effect via thorough inhibition of angiogenesis including RCCs [33,34]. Therefore, we chose *VEGFR2* as a therapeutic gene in this tumor model. The sequence of the anti *Vegfr2* siRNA was determined by comparing the gene silencing effect in cultured TECs (Fig. S10A). Then, OS-RC-2-bearing mice were daily injected twice with the most effective anti *Vegfr2* siRNA (si-*Vegfr2*) encapsulated in the RGD-MEND at a concentration of 3.0 mg/kg. As a result, a significant *Vegfr2* knockdown was observed *in vivo* (Fig. S10B). Additionally, si-*Vegfr2* had no effect on the viability of OS-RC-2 itself (Fig. S11). Then, when we monitored tumor growth after 3 injections of si-*Vegfr2* encapsulated in the RGD-MEND, a significant delay in tumor growth was observed (Fig. 6A). The si-*Vegfr2* treatment significantly lowered the amount

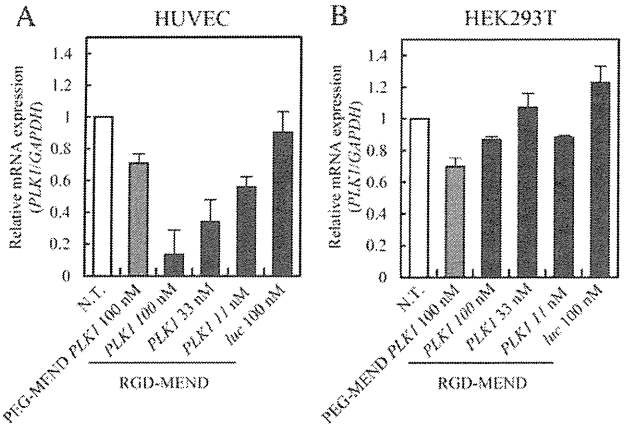

Fig. 3. Gene silencing effect of PEG-MEND and RGD-MEND. Cells were seeded on a 6-well plate 24 h prior to the MEND treatment, and the MENDs were then added to cells at the indicated concentrations for 24 h. Target gene mRNA expression was determined by qRT-PCR 24 h after the addition of PEG-MEND and RGD-MEND. *PLK1* expression was normalized to *GAPDH*.

of tumor wet tissue on day 17 compared to si-*luc* (Fig. 6B, C). To investigate whether *Vegfr2* suppression led to the inhibition of angiogenesis, vessels in tumor tissue were observed after 2 si-*Vegfr2* injections of 3.0 mg/kg by CLSM (Fig. 6D) The anti-angiogenesis effect was then evaluated by counting pixels indicating vessels; the vessels were significantly decreased in the si-*Vegfr2* group (Fig. 6E).

To evaluate the toxicity of systemically injected 3.0 mg/kg of RGD-MEND, we monitored changes in body weight during the treatment and also measured liver toxicity. No body weight change was observed in the OS-RC-2-bearing mice (Fig. 7A). Moreover, liposomal carriers sometimes severely injure the liver as liposomes tend to accumulate in liver. The activity of liver enzymes, AST and ALT, were not increased in the ICR mice at 24 h after the injection of 3.0 mg/kg MENDs (Fig. 7B).

4. Discussion

The cRGD peptide is a well-known ligand for both cancer cells and TECs. Although cRGD has been widely used as a targeting ligand for oligonucleotide delivery to TECs, there are few reports directly showing TEC-specific gene silencing mediated by siRNA. In this study, we verified that the RGD-MEND is capable of inducing siRNA-mediated gene silencing in TECs and attempted to develop a cancer therapy through an anti-angiogenic effect by delivering siRNA.

As previously described, the apparent pKa of the carrier is a dominant factor for escaping from endosomes in pH responsive carriers [10]. After internalization via endocytosis, the YSK-MEND is rapidly converted into a cationic molecule in response to acidification in the endosomes, and, consequently, the endosomal membrane is disrupted by interacting with endosomal membranes with a negative charge. Therefore, it is important to adjust the pKa of the particle to around 6.5 in order to rapidly respond the declining pH in endosomes. The apparent pKa of the RGD-MEND was compared with the RGD-modified MEND. As a result, the pKa was around 6.5 and remained unchanged as the result of the modification of RGD (Fig S2). This suggests that the RGD-MEND would be able to efficiently escape from the endosome in response to endosome acidification after internalization mediated by $\alpha_V\beta_3$ integrin–RGD interaction. Five mole percent (mol%) of RGD-modification resulted in the maximum cellular uptake in HUVEC cells, whereas additional RGD-modification had no further effect on uptake. This saturation might be due to fixed quantity of $\alpha_V\beta_3$ integrin present on HUVEC cells. In addition, it was previously reported that the PEGylation ratio in liposomes was, at most, 5.0 mol% [35]. Collectively, 5.0 mol% of RGD-PEG might be the optimized modification condition in both aspects of cells and siRNA carriers.

Table 2
Characteristics of the YSK-MENDs used in the in vivo experiments.

	RGD-MEND	PEG-MEND	conventional YSK-MEND
Lipid composition	YSK05/POPE/chol/PEG-DMG/RGD-PEG 50/25/25/3/5	YSK05/POPE/chol/PEG-DMG/PEG-DSPE 50/25/25/3/5	YSK05/DSPC/chol PEG-DSG 50/10/40/3
Diameter (nm)	115 ± 10	115 ± 17	105 ± 10
PdI	0.18 ± 0.01	0.21 ± 0.03	0.16 ± 0.04
ζ-potential (mV)	−18 ± 4	−18 ± 14	2.8 ± 1.4

The above mentioned properties on internalization via $\alpha_V\beta_3$ integrin and pH responsive fusiogenicity allows RGD-MEND to achieve a significant level of gene silencing in TECs at a dose of si-*Cd31* 4.0 mg/kg (Fig. 5). Nevertheless, gene silencing was saturated at 50% of N.T. In addition, two injections of 4.0 mg/kg of the RGD-MEND failed to drastically improve gene silencing (data not shown). This saturation might be caused by a limited distribution of the RGD-MEND in tumor tissue. When the distribution in tumor tissue was measured after systemic injection of the RGD-MEND, the fluorescence derived from the RGD-MEND was detected in approximately 80% of the TECs (Fig. S5). As the tumor vasculature is more heterogenous than normal tissue, blood flow is not sufficient in some parts of tumor vessels [36,37]. This heterogeneity in blood flow could lead to a limited distribution of the systemically delivered RGD-MEND.

As gene silencing in endothelial cells in normal organs would cause undesirable adverse effects, we determined the extent of accumulation in plasma, liver, spleen, kidney and lung by the RI-labeled not-PEGylated YSK-MEND (MEND), the PEG-MEND and the RGD-MEND containing RIs were injected into ICR mice, and the radio activity of these tissues were then measured (Fig. S7). Only the PEG-MEND showed a prolonged circulation time, while the others did not. Notably, a significant increased accumulation of RGD-MEND was observed in the spleen and lungs. The MEND accumulated most highly in the liver of three MENDs. The increased accumulation in the spleen can be attributed to platelets, which are abundant in the spleen. Platelets express $\alpha_{IIb}\beta_3$ integrin, which has a relatively similar structure to $\alpha_V\beta_3$ integrin [38]. As cRGD can also weakly bind to the $\alpha_{IIb}\beta_3$ integrin, the RGD-MEND may have accumulated in spleen. Though the mechanism responsible for the high accumulation of RGD-MEND in lungs is currently unclear, the cRGD conjugated oligopeptide–plasmid DNA complex also

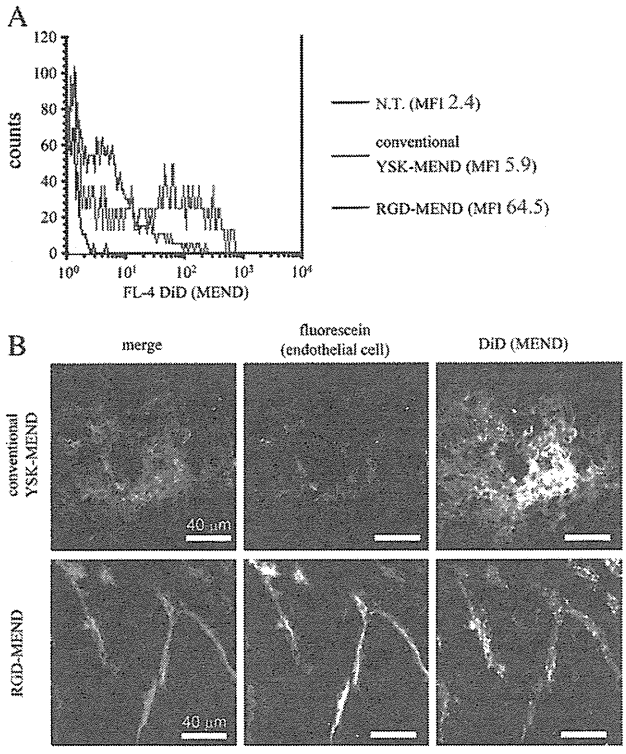

Fig. 4. Analysis of the localization of RGD-MEND in tumor tissue. Mean of the fluorescence intensity (MFI) of DiD in the CD31 positive population of tumor burden was compared among MENDs. B) DiD-labeled MENDs were injected into OS-RC-2-bearing mice, and 6 h after the injection, tumor tissues were collected and observed by CLSM. In merged images, green and red dots mean endothelial cells and MENDs, respectively. Upper panels show the images of conventional YSK-MEND and lower shows the images of RGD-MEND. Scale bars are 40 μm. N.T.: non treatment.

accumulated at slightly higher levels in the lungs compared to the un-modified version used in a previous report [39]. Thus, a modest higher accumulation in the lungs must be accompanied by cRGD modification. Taking into consideration the fact that the highest accumulation was in the liver and an increased accumulation was found in the lungs and spleen, *Cd31* gene silencing in these organs were evaluated 24 h after injection of the RGD-MEND. No significant gene reduction was observed in any of these organs (Fig. S9). Although a modestly higher accumulation of the RGD-MEND in the spleen and lungs was observed, there is little possibility that the systemic injection of RGD-MEND induced side effects in other organs. In the case of present anti-angiogenic agents, the inhibitory effect on angiogenesis in normal tissue, except for tumor tissue, can lead to an unfavorable influence. For example, Avastin can induce mortal side effects, such as bowel perforation and pulmonary hemorrhages because Avastin can inhibit VEGF signaling in normal tissue, which is required for the maintenance of healthy blood

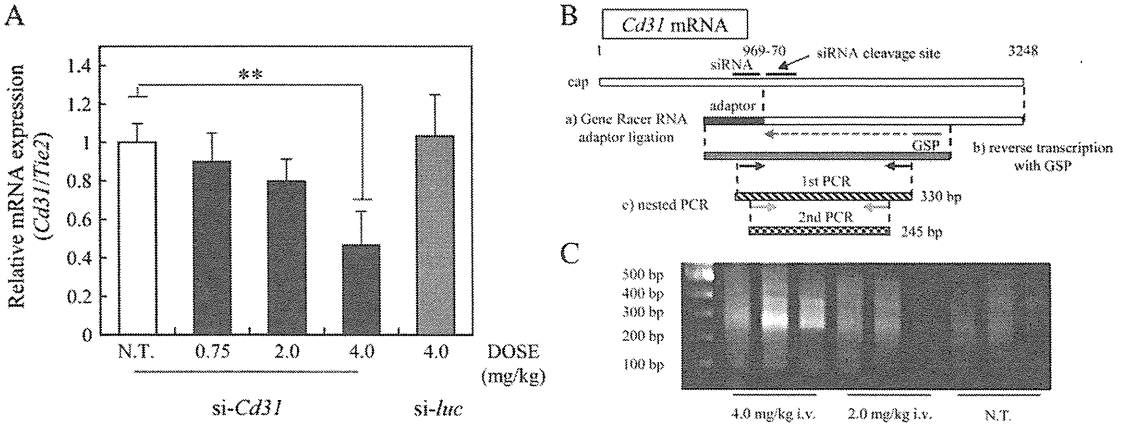

Fig. 5. Gene silencing via RNAi after injection of RGD-MEND. A) siRNA formulated in RGD-MEND was injected into OS-RC-2-bearing mice were injected at the indicated doses, and 24 h after the injection, *Cd31* expression was determined by qRT-PCR. B) Schematic diagram of the 5′ RACE-PCR method. Predicted cleavage site by si-*Cd31* was *Cd31* mRNA (3248 bp) and is indicated by an arrow between 969 and 970 bp of *Cd31 mRNA*. siRNA specific cleavage was detected as follows. First, the Gene Racer RNA adaptor was ligated into cleaved uncapped *Cd31* mRNA, and adaptor-ligated mRNA was then reverse transcribed with the gene specific primer (GSP). Next, complementary DNA was amplified by PCR with two independent primer sets (nested PCR). As a result, the production of 245 bp PCR fragment is indicative of siRNA-specific cleavage. C) The actual gel image of the 5′ RACE-PCR products. RNA extracted from tumor-bearing mice which were treated with 4.0 or 2.0 mg/kg siRNA encapsulated in RGD-MEND was subjected to a 5′ RACE-PCR procedure. N.T.: non treatment.

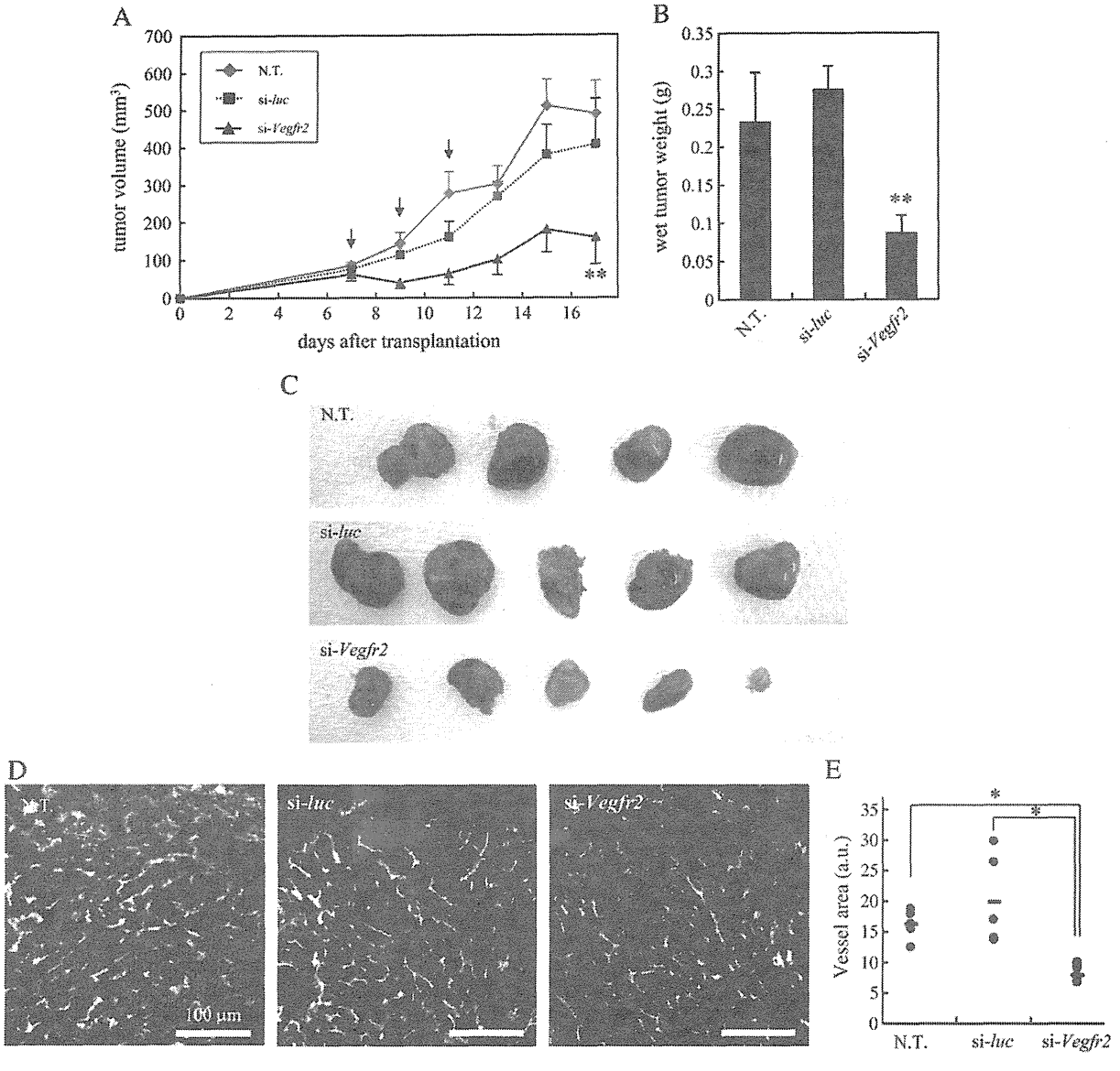

Fig. 6. Anti-tumor effect of si-*Vegfr2* encapsulated in RGD-MEND. A) RGD-MENDs encapsulating si-*luc* or si-*Vegfr2* were injected 3 times on alternate days at a dose of 3.0 mg/kg. Tumor volume was chronologically measured until day 17. Arrows denote the injection of the MEND. B) Wet tumor tissue was weighed when tumor was excised 17 days after transplantation. C) Photographs of collected tumor tissues. **: $p < 0.05$ (ANOVA followed by Bonferroni correction vs. N.T., $n = 5$). D) A typical image of each group is shown. Tumor bearing mice were injected with MENDs into tail vein twice. Twenty four hours after the injection, tumor tissues were excised and observed with CLSM. Scale bars are 100 μm. E) Pixels showing vessels, which were stained by isolectin B4, were counted with ImageJ. *; $p < 0.05$: ANOVA followed by SNK test, $n = 5–7$. N.T.: non treatment.

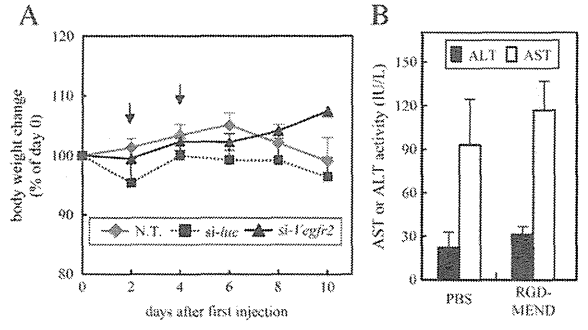

Fig. 7. Somatic and liver toxicological analyses of the RGD-MEND. A) The change in body weight was monitored after the first therapeutic injections into nude mice at a dose of 3.0 mg/kg every other day. Arrows show MENDs injection. B) Liver toxicity was evaluated by measuring the activities of selected liver enzymes, namely, ALT (black column) and AST (white column). These assays were performed 24 h after the injection of the RGD-MEND at a dose of 3.0 mg/kg. $n = 3$. N.T.: non treatment.

vessels [40,41]. In contrast, since the RGD-MEND could selectively suppress gene expression in tumor tissue, its use should be safer than the currently used anti-angiogenic agents.

Although OS-RC-2 cells were $\alpha_V\beta_3$ integrin positive (data not shown), no significant knockdown was observed in cancer cells (Fig. S8). The failure of cancer cell gene silencing was probably due to the lack of spreading of RGD-MEND in tumor tissue. Actually, almost all of the RGD-MEND appeared to remain in tumor vessels in the CLSM result (Fig. 5B). Although long-circulating liposomes can accumulate in tumor tissue after intravenous administration via the EPR effect as described above, the RGD-MEND failed to accumulate and diffuse in tumor tissue because of the instability of the RGD-MEND in the bloodstream (Fig. S7).

Although some groups reported on the therapeutic effect of cRGD itself, the injection of RGD-MEND encapsulating si-*luc* failed to inhibit tumor growth (Fig. 6A). In the reports dealing with the therapeutic effects of cRGD, the dosage of cRGD was 10–30 mg/kg [19,42,43]. On the other hand, the amount of cRGD was 1.6 mg/kg in the case of 4.0 mg/kg of cRGD-MEND. These facts suggest that the amount of cRGD on the RGD-MEND was insufficient to produce a curative effect. In contrast, tumor growth in the group treated with si-*Vegfr2* was markedly delayed. To exclude the possibility that si-*Vegfr2* led to cell death in OS-RC-2 cells themselves, we examined the effect of si-*Vegfr2* transfection to OS-RC-2 cells on viability. When OS-RC-2 cells were treated with si-*Vegfr2* and si-*luc*, no detectable reduction in cell viability compared to N.T. was found in both groups (Fig. S11). These results suggest that the injection of si-*Vegfr2* inhibits tumor growth via angiogenic gene knockdown in TECs.

5. Conclusions

The RGD-MEND caused significant gene silencing in tumor endothelial cells, but not in endothelial cells in normal organs and cancer cells without severe toxicity. In addition, 5′ RACE-PCR revealed that siRNA-mediated RNA interference was responsible for the gene reduction observed in TECs. In other words, we succeeded in developing an efficient system for the delivery of siRNA specifically to tumor endothelial cells. This system is a promising siRNA delivery system for investigations of the pathological characteristics of tumor endothelial cells, and moreover for cancer treatment via controlling of the biological function of tumor endothelial cells.

Grant support

This study was supported in part by a Grant-in-Aid for Research Activity Start-up (Grant Number 25893001), a Grant-in-Aid for Scientific Research on Innovative Areas "Nanomedicine Molecular Science" (No. 2306) from Ministry of Education, Culture, Sports, Science, and Technology (MEXT) of Japan, and the Special Education and Research Expenses of the Ministry of Education, Culture, Sports, Science and Technology (MEXT) of Japan.

Acknowledgments

The authors also wish to thank Dr. Milton S. Feather for his helpful advice in writing the English manuscript.

Appendix A. Supplementary data

Supplementary data to this article can be found online at http://dx.doi.org/10.1016/j.jconrel.2013.10.003.

References

[1] N. Ferrara, R.S. Kerbel, Angiogenesis as a therapeutic target, Nature 438 (2005) 967–974.
[2] L.M. Ellis, D.J. Hicklin, VEGF-targeted therapy: mechanisms of anti-tumour activity, Nat. Rev. Cancer 8 (2008) 579–591.
[3] J. Folkman, Tumor angiogenesis: therapeutic implications, N. Engl. J. Med. 285 (1971) 1182–1186.
[4] C. Harrison, Angiogenesis: a deeper understanding of VEGFR inhibitors, Nat. Rev. Cancer 12 (2012) 735.
[5] C. Harrison, Anticancer drugs: a deeper understanding of VEGFR inhibitors, Nat. Rev. Drug Discov. 11 (2012) 831.
[6] K.A. Whitehead, R. Langer, D.G. Anderson, Knocking down barriers: advances in siRNA delivery, Nat. Rev. Drug Discov. 8 (2009) 129–138.
[7] G.R. Rettig, M.A. Behlke, Progress toward *in vivo* use of siRNAs-II, Mol. Ther. 20 (2012) 483–512.
[8] K. Kogure, H. Akita, Y. Yamada, H. Harashima, Multifunctional envelope-type nano device (MEND) as a non-viral gene delivery system, Adv. Drug Deliv. Rev. 60 (2008) 559–571.
[9] H. Hatakeyama, H. Akita, H. Harashima, A multifunctional envelope type nano device (MEND) for gene delivery to tumours based on the EPR effect: a strategy for overcoming the PEG dilemma, Adv. Drug Deliv. Rev. 63 (2011) 152–160.
[10] Y. Sato, H. Hatakeyama, Y. Sakurai, M. Hyodo, H. Akita, H. Harashima, A pH-sensitive cationic lipid facilitates the delivery of liposomal siRNA and gene silencing activity *in vitro* and *in vivo*, J. Control. Release 163 (2012) 267–276.
[11] Y. Sakurai, H. Hatakeyama, Y. Sato, M. Hyodo, H. Akita, H. Harashima, Gene silencing via RNAi and siRNA quantification in tumor tissue using MEND, a liposomal siRNA delivery system, Mol. Ther. 2 (2013) 1195–1203.
[12] A.D. Judge, M. Robbins, I. Tavakoli, J. Levi, L. Hu, A. Fronda, E. Ambegia, K. McClintock, I. MacLachlan, Confirming the RNAi-mediated mechanism of action of siRNA-based cancer therapeutics in mice, J. Clin. Invest. 119 (2009) 661–673.
[13] S.C. Semple, A. Akinc, J. Chen, A.P. Sandhu, B.L. Mui, C.K. Cho, D.W. Sah, D. Stebbing, E.J. Crosley, E. Yaworski, I.M. Hafez, J.R. Dorkin, J. Qin, K. Lam, K.G. Rajeev, K.F. Wong, L.B. Jeffs, L. Nechev, M.L. Eisenhardt, M. Jayaraman, M. Kazem, M.A. Maier, M. Srinivasulu, M.J. Weinstein, Q. Chen, R. Alvarez, S.A. Barros, S. De, S.K. Klimuk, T. Borland, V. Kosovrasti, W.L. Cantley, Y.K. Tam, M. Manoharan, M.A. Ciufolini, M.A. Tracy, A. de Fougerolles, I. MacLachlan, P.R. Cullis, T.D. Madden, M.J. Hope, Rational design of cationic lipids for siRNA delivery, Nat. Biotechnol. 28 (2010) 172–176.
[14] M. Meyer, A. Philipp, R. Oskuee, C. Schmidt, E. Wagner, Breathing life into polycations: functionalization with pH-responsive endosomolytic peptides and polyethylene glycol enables siRNA delivery, J. Am. Chem. Soc. 130 (2008) 3272–3273.
[15] H. Yu, Y. Zou, Y. Wang, X. Huang, G. Huang, B.D. Sumer, D.A. Boothman, J. Gao, Overcoming endosomal barrier by amphotericin B-loaded dual pH-responsive PDMA-b-PDPA micelleplexes for siRNA delivery, ACS Nano 5 (2011) 9246–9255.
[16] V.P. Torchilin, Recent advances with liposomes as pharmaceutical carriers, Nat. Rev. Drug Discov. 4 (2005) 145–160.
[17] C.J. Avraamides, B. Garmy-Susini, J.A. Varner, Integrins in angiogenesis and lymphangiogenesis, Nat. Rev. Cancer 8 (2008) 604–617.
[18] C. Mas-Moruno, F. Rechenmacher, H. Kessler, Cilengitide: the first anti-angiogenic small molecule drug candidate design, synthesis and clinical evaluation, Anticancer Agents Med. Chem. 10 (2010) 753–768.
[19] P.C. Brooks, A.M. Montgomery, M. Rosenfeld, R.A. Reisfeld, T. Hu, G. Klier, D.A. Cheresh, Integrin alpha v beta 3 antagonists promote tumor regression by inducing apoptosis of angiogenic blood vessels, Cell 79 (1994) 1157–1164.
[20] F. Danhier, A. Le Breton, V. Preat, RGD-based strategies to target alpha(v) beta(3) integrin in cancer therapy and diagnosis, Mol. Pharm. 9 (2012) 2961–2973.
[21] R.J. Christie, Y. Matsumoto, K. Miyata, T. Nomoto, S. Fukushima, K. Osada, J. Halnaut, F. Pittella, H.J. Kim, N. Nishiyama, K. Kataoka, Targeted polymeric micelles for siRNA treatment of experimental cancer by intravenous injection, ACS Nano 6 (2012) 5174–5189.
[22] E. Kenjo, T. Asai, N. Yonenaga, H. Ando, T. Ishii, K. Hatanaka, K. Shimizu, Y. Urita, T. Dewa, M. Nango, H. Tsukada, N. Oku, Systemic delivery of small interfering RNA by use of targeted polycation liposomes for cancer therapy, Biol. Pharm. Bull. 36 (2013) 287–291.
[23] T. Tagami, T. Suzuki, M. Matsunaga, K. Nakamura, N. Moriyoshi, T. Ishida, H. Kiwada, Anti-angiogenic therapy via cationic liposome-mediated systemic siRNA delivery, Int. J. Pharm. 422 (2012) 280–289.
[24] S. Anand, B.K. Majeti, L.M. Acevedo, E.A. Murphy, R. Mukthavaram, L. Scheppke, M. Huang, D.J. Shields, J.N. Lindquist, P.E. Lapinski, P.D. King, S.M. Weis, D.A. Cheresh, MicroRNA-132-mediated loss of p120RasGAP activates the endothelium to facilitate pathological angiogenesis, Nat. Med. 16 (2010) 909–914.
[25] D.Y. Heng, R.M. Bukowski, Anti-angiogenic targets in the treatment of advanced renal cell carcinoma, Curr. Cancer Drug Targets 8 (2008) 676–682.
[26] B. Escudier, Emerging immunotherapies for renal cell carcinoma, Ann. Oncol. 23 (Suppl. 8) (2012) viii35–viii40.
[27] G. Bergers, D. Hanahan, Modes of resistance to anti-angiogenic therapy, Nat. Rev. Cancer 8 (2008) 592–603.
[28] J.S. Ko, P. Rayman, J. Ireland, S. Swaidani, G. Li, K.D. Bunting, B. Rini, J.H. Finke, P.A. Cohen, Direct and differential suppression of myeloid-derived suppressor cell subsets by sunitinib is compartmentally constrained, Cancer Res. 70 (2010) 3526–3536.
[29] I. Helfrich, I. Scheffrahn, S. Bartling, J. Weis, V. von Felbert, M. Middleton, M. Kato, S. Ergun, D. Schadendorf, Resistance to antiangiogenic therapy is directed by vascular phenotype, vessel stabilization, and maturation in malignant melanoma, J. Exp. Med. 207 (2010) 491–503.
[30] G. Kibria, H. Hatakeyama, N. Ohga, K. Hida, H. Harashima, Dual-ligand modification of PEGylated liposomes shows better cell selectivity and efficient gene delivery, J. Control. Release 153 (2011) 141–148.
[31] N. Ohga, K. Hida, Y. Hida, C. Muraki, K. Tsuchiya, K. Matsuda, Y. Ohiro, Y. Totsuka, M. Shindoh, Inhibitory effects of epigallocatechin-3 gallate, a polyphenol in green tea, on tumor-associated endothelial cells and endothelial progenitor cells, Cancer Sci. 100 (2009) 1963–1970.

[32] H. Maeda, Y. Matsumura, H. Kato, Purification and identification of [hydroxyprolyl3] bradykinin in ascitic fluid from a patient with gastric cancer, J. Biol. Chem. 263 (1988) 16051–16054.
[33] R.A. Brekken, J.P. Overholser, V.A. Stastny, J. Waltenberger, J.D. Minna, P.E. Thorpe, Selective inhibition of vascular endothelial growth factor (VEGF) receptor 2 (KDR/Flk-1) activity by a monoclonal anti-VEGF antibody blocks tumor growth in mice, Cancer Res. 60 (2000) 5117–5124.
[34] I.J. Duignan, E. Corcoran, A. Pennello, M.J. Plym, M. Amatulli, N. Claros, M. Iacolina, H. Youssoufian, L. Witte, S. Samakoglu, J. Schwartz, D. Surguladze, J.R. Tonra, Pleiotropic stromal effects of vascular endothelial growth factor receptor 2 antibody therapy in renal cell carcinoma models, Neoplasia 13 (2011) 49–59.
[35] K. Sou, T. Endo, S. Takeoka, E. Tsuchida, Poly(ethylene glycol)-modification of the phospholipid vesicles by using the spontaneous incorporation of poly(ethylene glycol)-lipid into the vesicles, Bioconjug. Chem. 11 (2000) 372–379.
[36] P. Vaupel, F. Kallinowski, P. Okunieff, Blood flow, oxygen and nutrient supply, and metabolic microenvironment of human tumors: a review, Cancer Res. 49 (1989) 6449–6465.
[37] A.R. Pries, A.J. Cornelissen, A.A. Sloot, M. Hinkeldey, M.R. Dreher, M. Hopfner, M.W. Dewhirst, T.W. Secomb, Structural adaptation and heterogeneity of normal and tumor microvascular networks, PLoS Comput. Biol. 5 (2009) e1000394.
[38] F. Bianchini, N. Cini, A. Trabocchi, A. Bottoncetti, S. Raspanti, E. Vanzi, G. Menchi, A. Guarna, A. Pupi, L. Calorini, (1)(2)(5)I-radiolabeled morpholine-containing arginine-glycine-aspartate (RGD) ligand of alphavbeta(3) integrin as a molecular imaging probe for angiogenesis, J. Med. Chem. 55 (2012) 5024–5033.
[39] Y. Aoki, S. Hosaka, S. Kawa, K. Kiyosawa, Potential tumor-targeting peptide vector of histidylated oligolysine conjugated to a tumor-homing RGD motif, Cancer Gene Ther. 8 (2001) 783–787.
[40] T. Eisen, C.N. Sternberg, C. Robert, P. Mulders, L. Pyle, S. Zbinden, H. Izzedine, B. Escudier, Targeted therapies for renal cell carcinoma: review of adverse event management strategies, J. Natl. Cancer Inst. 104 (2012) 93–113.
[41] S. Goel, D.G. Duda, L. Xu, L.L. Munn, Y. Boucher, D. Fukumura, R.K. Jain, Normalization of the vasculature for treatment of cancer and other diseases, Physiol. Rev. 91 (2011) 1071–1121.
[42] F. Mitjans, T. Meyer, C. Fittschen, S. Goodman, A. Jonczyk, J.F. Marshall, G. Reyes, J. Piulats, *In vivo* therapy of malignant melanoma by means of antagonists of alphav integrins, Int. J. Cancer 87 (2000) 716–723.
[43] M.A. Buerkle, S.A. Pahernik, A. Sutter, A. Jonczyk, K. Messmer, M. Dellian, Inhibition of the alpha-nu integrins with a cyclic RGD peptide impairs angiogenesis, growth and metastasis of solid tumours *in vivo*, Br. J. Cancer 86 (2002) 788–795.

Journal of Controlled Release 173 (2014) 43–50

Contents lists available at ScienceDirect

Journal of Controlled Release

journal homepage: www.elsevier.com/locate/jconrel

The systemic administration of an anti-miRNA oligonucleotide encapsulated pH-sensitive liposome results in reduced level of hepatic microRNA-122 in mice

Hiroto Hatakeyama [a], Manami Murata [a], Yusuke Sato [a], Mayumi Takahashi [a], Noriaki Minakawa [b], Akira Matsuda [a], Hideyoshi Harashima [a,*]

[a] Faculty of Pharmaceutical Sciences, Hokkaido University, Sapporo, Hokkaido, 060-0812, Japan
[b] Graduate School of Pharmaceutical Sciences, The University of Tokushima, Tokushima, Japan

ARTICLE INFO

Article history:
Received 5 August 2013
Accepted 18 October 2013
Available online 25 October 2013

Keywords:
miRNA
Antisense oligonucleotide
Drug delivery system
Liposomes
miR-122

ABSTRACT

Efficient delivery continues to be a challenge in microRNA (miRNA) therapeutics. We utilized a pH-sensitive multifunctional envelope-type nano device (MEND) containing a pH-sensitive lipid YSK05 (YSK05-MEND) to regulate liver specific miRNA-122 (miR-122). Anti-microRNA oligonucleotides including 2′-OMe and phosphorothioate modifications against miR-122 (AMO122) were encapsulated in the YSK05-MEND. Despite the lower uptake, the YSK05-MEND showed a higher activity in liver cancer cells than Lipofectamine2000 (LFN2k) due to efficient endosomal escape. Cytotoxicity was minimal at 100 nM of AMO122 in YSK05-MEND treated cells, but LFN2k showed toxicity at 50 nM. When mice were administrated with free AMO122, it was eliminated *via* the kidney due to its molecular weight, and lesser amounts were detected in the liver. Conversely, the YSK05-MEND delivered higher amounts of the AMO122 to the liver. Systemic administration of YSK05-MEND induced the knockdown of miR-122 and an increase in target genes in the liver, and a subsequent reduction in plasma cholesterol at a dose of 1 mg AMO/kg while free AMO122 showed no activity at the same dose. The effect of AMO122 delivered by YSK05-MEND persisted for over 2 weeks. These results suggest that YSK05-MEND is a promising system for delivering AMOs to the liver.

1. Introduction

MicroRNAs (miRNAs) are a class of small non-coding RNAs (~22 nt) that regulate gene expression by binding to the 3′-untranslated region (3′-UTR) of target genes, triggering the degradation of messenger RNA (mRNA) or the inhibition of protein translation [1]. MicroRNA-122 (miR-122) is a conserved liver-specific miRNA that accounts for 70% of the total miRNA population [2] and plays important roles in liver physiology, such as lipid metabolism [3,4], diseases in hepatic virus C (HCV) infections [5] and hepatocellular carcinoma (HCC) [6]. In addition, the expression of miR-122 in other organs such as heart is negligible [7]. Thus, miR-122 is an attractive and selective therapeutic target for the treatment of liver diseases [8].

A number of attempts have been made to induce the specific inhibition of endogenous miRNAs *in vivo*. Plasmid DNA vectors that express miRNA sponges, which contain multiple tandem miRNA binding sites, have been designed to competitively inhibit miRNA functions in mammalian cells [9]. It was recently reported that the intravenous administration of recombinant adeno associated virus (rAAV) vectors with miRNA tough decoys (TuDs) result in reduced levels of miR-122 and serum cholesterol [10]. Anti-microRNA oligonucleotides (anti-miRs) have been widely employed to inhibit miRNAs, including a variety of nucleoside modifications, such as 2′-O-methyl (2′-OMe), 2′-O-methoxyethyl (2′-MOE), and locked nucleic acid (LNA) was developed in an attempt to enhance binding affinity to target miRNAs with phosphorothioate (PS) linkages to improve nuclease resistance [11]. The systemic injection of these anti-miRs against miR-122 (anti-miR122) into mice resulted in a reduction in cholesterol levels [3,4,12–14]. Miravirsen, an LNA-modified anti-miR122, is currently in phase 2 clinical trials for the treatment of HCV [15].

However, large doses of anti-miR-122 are required to induce the phenotype when the free form of anti-miR-122 is injected due to renal excretion and poor tissue selectivity as well as cellular uptake [16–18]. To overcome these issues, systems that are capable of delivering nucleic acids to a targeted organ are desired [18]. Lipid based nanoparticles have been extensively investigated as vehicles for delivering siRNAs, miRNAs, as well as anti-miRs [19–23]. We developed a multifunctional envelope-type nano device (MEND), in which nucleic acids are encapsulated within a lipid envelope [24,25]. We recently synthesized a pH-sensitive cationic lipid, referred to as YSK05 [26]. A MEND composed of YSK05 (YSK05-MEND) showed efficient pH-sensitive fusogenic properties and a higher gene knockdown ability than a commercially available transfection reagent, Lipofectamine 2000 (LFN2k) in HeLa cells

* Corresponding author. Tel.: +81 11 706 3919; fax: +81 11 706 4879.
E-mail address: harasima@pharm.hokudai.ac.jp (H. Harashima).

0168-3659/$ – see front matter © 2013 Elsevier B.V. All rights reserved.
http://dx.doi.org/10.1016/j.jconrel.2013.10.023

[26]. The systemic administration of YSK05-MEND modified with PEG delivered siRNA to tumor tissue in renal cell carcinoma xenograft mice *via* the enhanced permeability and retention (EPR) effect and induced the knockdown of approximately 50% of the target gene at a dose of 3 mg/kg body weigh [27]. These findings indicate that YAK05-MEND has the potential for use in nucleic acid delivery both *in vitro* and *in vivo*.

In the present study, we report on an investigation of whether the YSK05-MEND could be applicable for use in an anti-miR-122 delivery system to murine liver. We first evaluated the physical properties of the YSK05-MEND encapsulating anti-miR-122 modified with 2′-OMe and PS linkages (AMO122) and its activity in murine hepatoma cells in comparison with LFN2k. For *in vivo* studies, we compared the activity of systemically administrated YSK05-MEND with free AMO in terms of distribution in the liver and kidney, and the effect of antagonism of target miR-122 on the increase in the expression level of genes that are regulated by miR-122 and the subsequent reduction in plasma cholesterol levels. The findings indicate that the YSK05-MEND has the potential for use in the efficient delivery of AMOs to murine liver.

2. Materials and methods

2.1. Materials

Cholesterol (Chol) was purchased from AVANTI Polar Lipids (Alabaster, AL, USA). 1,2-Dimyristoyl-*sn*-glycerol-methoxypolyethyleneglycol 2000 ether (PEG-DMG) was purchased from NOF Corporation (Tokyo, Japan). YSK05 was synthesized as described previously [26]. Anti-miR against miR-122 (AMO122) (5′-$A_sC_sA_sA_sA_sC_sA_sC_sC_sA_sU_sU_sG_sU_s$ $C_sA_sC_sA_sC_sU_sC_sC_sA$-3′) and Cy5-labeled AMO (Cy5-AMO) (5′-Cy5-A_sC_s GAUAAACGGUUGUCUACG$_sU_sC_sA_s$-3′) were purchased from Hokkaido System Science Co., Ltd. (Sapporo, Japan) (2′-OMe-modified nucleotides; subscript 's' represents a phosphorothioate linkage). Quant-iT RiboGreen RNA assay was purchased from Molecular Probes (Eugene, OR, USA). MEM alpha, Lipofectamine 2000 (LF2k) and TRIzol were purchased from Invitrogen (Carlsbad, CA, USA). Taqman MicroRNA Reverse Transcription Kit, TaqMan microRNA assay kit, High Capacity RNA-to-cDNA kit, and Fast SYBR Green Master Mix were obtained from Applied Biosystems (Foster City, CA). Amicon Ultra (MWCO 100 K) was obtained from Millipore (Bedford, MA, USA). Murine hepatoma Hepa1c1c7 cells obtained from American Type Culture Collection (ATCC, Manassas, VA, USA).

2.2. Preparation of the YSK05-MEND encapsulating AMO122 (AMO122-YSK05-MEND)

The YSK05-MEND was prepared with the pH-sensitive cationic lipid YSK05, cholesterol and PEG-DMG (molar ratio: 70/30/3) using a *t*-BuOH dilution method. The lipid in 90% (v/v) *t*-BuOH was mixed with AMO122 in 20 mM citrate buffer (pH 4.0) at an AMO/lipid ratio of 0.1 (wt/wt) under strong agitation to a *t*-BuOH concentration of 60% (v/v). The lipid/AMO122 mixture was then added to 20 mM citrate buffer (pH 4.0) under strong agitation to a *t*-BuOH concentration of <12% (v/v). Ultrafiltration was performed using Amicon Ultra for removing *t*-BuOH, replacing external buffer with phosphate buffered saline (PBS, pH 7.4) and concentrating AMO122-YSK05-MEND.

2.3. Characterization of AMO122-YSK05-MEND

The average diameter, polydispersity index (pdi) and zeta-potential of AMO122-YSK05-MEND were determined using a Zetasizer Nano ZS ZEN3600 (MALVERN Instrument, Worchestershire, UK). AMO122 encapsulation efficiency was determined by RiboGreen assay [26]. AMO122-YSK05-MEND was diluted in 10 mM hepes buffer (pH7.4) containing 20 μg/ml dextran sulfate and Ribogreen in the presence or absence of 0.1 w/v% Triton X-100. Fluorescence was measured by a Varioskan Flash (Thermo scientific, Waltham, MA, USA) with λex = 500 nm, λem = 525 nm. AMO122 concentration was calculated from AMO122 standard curve. AMO122 encapsulation efficiency was calculated by comparing the AMO122 concentration in the presence and absence of Triton X-100. Free AMO122 and AMO122-YSK05-MEND including 1.2 μg AMO122 in the presence and absence of 20 μg/ml dextran sulfate and 0.1 w/v% Triton X-100 were electrophoresed through a 2.5% agarose gel at 100 V for 20 min and then stained with ethidium bromide and visualized under UV light using an Image Quant LAS4000 (GE healthcare, Piscataway, NJ, USA). The pH-sensitivity of AMO122-YSK05-MEND was determined using 6-(*p*-toluidino)-2-naphthalenesulfonic acid (TNS) (Wako, Osaka, Japan) [26]. 30 μM of lipid of AMO122-YSK05-MEND and 6 μM of TNS were mixed in 200 μl of 20 mM citrate buffer, 20 mM sodium phosphate buffer, or 20 mM Tris–HCl buffer, containing 130 mM NaCl at a pH ranging from 3.0 to 9.0. Fluorescence was measured by a Varioskan Flash with λex = 321 nm, λem = 447 nm, at 37 °C. The highest fluorescence was relatively assigned value of 1. The curve fitting was accomplished using Sigmaplot 12 (Hulinks, Tokyo, Japan). The pKa values were measured using the fitting curve as the pH giving rise to half-maximal fluorescent intensity.

2.4. In vitro transfection of AMO122 into hepatocytes and RNA isolation

Hepa1c1c7 cells were cultured in cell-culture dishes (Corning, New York, NY, USA) containing MEM alpha supplemented with 10% fetal bovine serum, penicillin (100 U/ml) and streptomycin (100 mg/ml) at 37 °C in an atmosphere of 5% CO_2 and 95% humidity. One day prior to the transfection of AMO, 2.5×10^4 Hepa1c1c7 cells were seeded in 6-well plates. AMO122-YSK05-MEND was diluted by MEM alpha supplemented with 10% fetal bovine serum (FBS). The cells were washed by PBS (pH 7.4), then 1.5 ml of MEM alpha containing AMO122-YSK05-MEND at the indicated concentration of AMO122 was added to the wells, followed by incubation at 37 °C for 48 h. LFN2k was used as a control, according to the manufacturer's protocol. The cells were washed twice with 1 ml PBS. Total RNA was extracted with TRIzol reagent according to the manufacturer's instructions. To evaluate cytotoxicity, cells were washed twice with PBS at 48 h, then incubated with 400 μl of Passive Lysis Buffer (Promega, Madison, WI, USA), followed by centrifugation (12,000 rpm, 4 °C, 5 min). Protein concentration in the supernatant was determined using BCA Protein Assay Kit (PIERCE, Rockford, IL). Phase-contrast images of the diluted sample were captured using a phase-contrast microscope (CKX41, OLYMPUS, Tokyo, Japan).

2.5. Reverse transcription (RT) and real-time PCR for miRNA and mRNA quantification

Mature miRNA-122 expression was determined using a Taqman MicroRNA Reverse Transcription Kit according to the manufacturer recommended protocols. Briefly, 100 ng of isolated RNA, 0.5 μl of stem-loop RT primer, RT buffer, 1 mM deoxyribonucleoside triphosphate mix, 3.35 units/μl MultiScribe reverse transcriptase, and 0.26 units/μl RNase inhibitor were used in 10 μl RT reactions for 30 min at 16 °C, 30 min at 42 °C, and 5 min at 85 °C. Complementary DNA was then subjected to real-time PCR using a TaqMan™ microRNA assay kit. The 15 μl reaction volume included 5 μl of cDNA (1:60 dilution), 0.75 μl of primer, and 7.5 μl of TaqMan Universal PCR Master Mix reactions was processed in Lightcycler480 system II (Roche) as follows: for 10 min at 95 °C (denaturation) and 40 cycles of 15 s at 95 °C and 1 min at 60 °C (annealing/extension). miRNA expression was calculated using ΔΔCt method being normalized to small nuclear RNA (snRNA) RNU6B.

For the determination of mRNA, 1.0 μg of isolated RNA was reverse transcribed using a High Capacity RNA-to-cDNA kit according to the manufacturer's instructions as described previously [27]. A quantitative PCR analysis was performed on 20 ng of cDNA using Fast SYBR Green Master Mix and Lightcycler480 system II. All reactions were performed at a volume of 15 μl. The PCR was processed in Lightcycler480 system II

as follows: for 20 s at 95 °C (denaturation) and 40 cycles of 3 s at 95 °C and 30 s at 60 °C for 30 s (annealing/extension). The amount of target gene was calculated using the ΔΔCt method normalized to hypoxanthine phosphoribosyltransferase 1 (*Hprt1*) mRNA. The primers for murine aldolase A (*Aldoa*) were (forward) 5′-GATGGGTCCAGCT TCAAC-3′ and (reverse) 5′-GTGCTTTCCTTTCCTAACTCTG-3′, branched-chain ketoacid dehydrogenase (*Bckdk*) were (forward) 5′-AGGACCT ATGCATGGCTTTG-3′ and (reverse) 5′-CCGTAGGTAGACATCCGTG-3′, N-myc downstream regulated gene 3 (*Ndrg3*) were (forward) 5′-ATGGGCTACATACCATCTGC-3′ and (reverse) 5′-TCTGACTGATTGCT GGTCAC-3′ and *Hprt1* were (forward) 5′-CGTGATTAGCGATGATGAAC-3′ and (reverse) 5′-GCAAGTCTTTCAGTCCTGTC-3′.

2.6. Determination of cellular uptake of Cy5-AMO encapsulated YSK05-MEND

One day prior to the transfection of Cy5-AMO, Hepa1c1c7 cells were seeded at a density of 1.5×10^5 cells per well in 6-well plates (Corning). Cy5-AMO encapsulated YSK05-MEND was diluted with MEM alpha containing 10% FBS, followed by the incubation with cells for 2 h at 20 nM of AMO. The cells with incubated with LFN2k complexed with Cy5-AMO in MEM alpha for 2 h at 20 nM of AMO, according to the manufacture's protocol. The cells were washed with 1 ml PBS, and detached by treatment with 0.05% trypsin-PBS. The cells were kept in ice and evaluated on a FACSCalibur flow cytometer (BD Biosciences, San Diego, CA, USA). The results were analyzed using Cell-Quest (BD Biosciences).

2.7. Observation of intracellular trafficking of Cy5-AMO encapsulated MEND

One day prior to transfection, 1.5×10^5 Hepa1c1c7 cells were seeded in a 35-mm glass-bottom dish (Iwaki, Osaka, Japan) in 1.5 ml of medium. YSK05-MEND or LFN2k containing Cy5-AMO was added at 100 nM of AMO concentration, followed by incubation at 37 °C for 1 h. The cells were washed twice with 1 ml of PBS, and were then fixed with 4% paraformaldehyde (PFA)-PBS for 10 min. The fixed cells were stained with Hoechst 33342 (Wako, Osaka, Japan) for 10 min. The cells were washed twice with 1 ml of PBS. The cells were added to Krebs Henseleit buffer and images were captured with a FLUOVIEW FV10i confocal microscope (OLYMPUS, Tokyo, Japan) equipped with a ×60 water objective lens.

2.8. In vivo experiments

Female ICR mice (7–8 weeks old) were purchased from Japan SLC (Shizuoka, Japan). One day prior to administration (day −1), blood was collected to determine cholesterol and alanine aminotransferase (ALT) levels. Either free AMO122 or AMO122-YSK05-MEND at a dose of 1 mg/kg AMO122 in a total volume of 10–15 ml/kg was intravenously administered to mice *via* the tail vein at days 0, 2 and 4. At the indicated times after the administration, the blood and liver were collected. Blood sample was centrifuged at 8 *g* at 4 °C for 5 min to obtain plasma. To obtain serum, blood samples were stored overnight at 4 °C, followed by centrifugation (10,000 rpm, 4 °C, 10 min). Cholesterol in plasma and ALT levels in serum were determined by a Cholesterol *E*-test WAKO and Transaminase CII-test WAKO (Wako, Osaka, Japan), respectively according to manufacturer recommended protocols. Liver tissue was homogenized in TRIzol using a PreCellys (Bertin Technologies, France). The total RNA in the supernatant was then isolated following the manufacturer's instructions. Target miRNA and mRNA levels were determined as described above. For histological observation, either free Cy5-AMO or YSK05-MEND encapsulating Cy5-AMO was intravenously administered to mice *via* the tail vein at a dose of 1 mg/kg AMO. At 30 min after administration, each animal was perfused with PBS to remove blood from the liver, which was then collected and fixed in 4% PFA-PBS for 24 h. The liver was sectioned into 150 μm thick sections using a super microslicer ZERO1 (Dosaka, Kyoto, Japan), and nuclei were stained by Hoechst33342. Images were captured using a Nikon A1 confocal microscope (Nikon, Tokyo, Japan) equipped with a ×60 water objective lens. Kidney tissue stained by Hoechst33342 was imaged by Nikon A1 equipped with a ×40 dry objective lens. The experimental protocols were reviewed and approved by the Hokkaido University Animal Care Committee in accordance with the "Guide for the Care and Use of Laboratory Animals".

2.9. Statistical analysis

Comparisons between multiple treatments were made using one-way analysis of variance (ANOVA), followed by the SNK test. Pair-wise comparisons between treatments were made using a Student's *t*-test. A P-value of <0.05 was considered as significant difference.

3. Results

3.1. Characterization of the prepared AMO122-YSK05-MEND

The average diameter, pdi and zeta-potential of the AMO122-YSK05-MEND were 71 ± 2 nm, 0.20 ± 0.01 and 3.1 ± 0.5 mV, respectively. The characteristics of empty YSK05-MEND prepared by the same procedure without AMO122 were similar (72 ± 2 d. nm, pdi 0.24 ± 0.02, zeta-potential 7.3 ± 1.2 mV). The recovery and encapsulation efficiency of AMO122 determined with RiboGreen were 91 ± 6% and 99 ± 1%, respectively. The encapsulation of AMO122 was also confirmed by electrophoresis (Fig. S1a). The apparent pKa of AMO122-YSK05-MEND was determined to be approximately 6.6, indicating that the YSK05-MEND could be converted into a cationic species in early endosomes (Fig. S1b).

3.2. Determination of the in vitro expression of miR-122 targeted genes and cytotoxicity

It has been reported that *Aldoa* is regulated by miR-122, and the inhibition of miR-122 leads to an increase in the expression level of *AldoA* [3,4]. Therefore, we first determined the expression level of *Aldoa* by qRT-PCR after the AMO122-YSK05-MEND treatment in comparison with a commercially available reagent, LFN2k [5,28]. The use of the AMO122-YSK05-MEND caused an increase in the expression of *Aldoa* in a dose-dependent manner, and the enhancement by AMO122-YSK05-MEND was higher than that for LFN2k/AMO122 complex (717 ± 68 d. nm, pdi 0.43 ± 0.09, zeta-potential 27.1 ± 4.0 mV) (Fig. 1a). Even though the AMO122-YSK05-MEND showed no cytotoxicity up to 100 nM of AMO122, LFN2k showed cytotoxicity at more than 50 nM of AMO, which can be attributed to the potent cationic charge of LFN2k (Fig. 1b and c).

The uptake amount of Cy5-labeled AMO (Cy5-AMO) formulated in the YSK05-MEND and LFN2k was assessed by flow cytometry. LFN2k. A heterogeneous cellular uptake of Cy5-AMO was observed in the case of LFN2k. On the other hand, Cy5-AMO was homogenously taken up by cells that had been treated with YSK05-MEND (Fig. 2a). Despite the higher activity (Fig. 1a), the relative mean fluorescent intensity of the YSK05-MEND treated cells was around 2 fold less than that for LFN2k (Fig. 2b). Intracellular observations indicated that aggregated forms of Cy5-AMO were produced when LFN2k was used, but diffused pattern was found in the case of YSK05-MEND (Fig. 2c). These findings suggest that Cy5-AMOs formulated in LFN2k becomes trapped in endosomes/lysosomes or in vesicular compartments. On the other hand, Cy5-AMOs encapsulated in YSK05-MEND was able to efficiently escape from endosomes. These results indicate that a pH-sensitive MEND composed of YSK05 induced the efficient inhibition of miRNA by delivering AMO to the cytosol and subsequently increasing the expression of the target genes.